

Outer and inner mass distributions of the irregular galaxies UGC 4284 and UGC 11861: Constraining the baryonic content through stellar population synthesis studies

P. Repetto^{1*}, Eric E. Martínez-García², M. Rosado³, R. Gabbasov⁴

¹*Laboratório Nacional de Astrofísica, Rua Estados Unidos 154, 37504-364, Itajubá, MG, Brazil*

²*Instituto Nacional de Astrofísica Óptica y Electrónica, Luis Enrique Erro 1, Tonantzintla, Puebla, México C.P. 72840*

³*Instituto de Astronomía, Universidad Nacional Autónoma de México, Circuito de la Investigación Científica, Ciudad Universitaria, México, D.F., C.P. 04510*

⁴*Instituto de Ciencias Básicas e Ingenierías, U.A.E.H., Carretera Pachuca-Tulancingo, México, C.P. 42184*

ABSTRACT

In this article we investigate the outer and inner mass distributions of the irregular galaxies UGC 4284 and UGC 11861, taking advantage of published HI and H α high resolution rotation curves and constraining the stellar disk of both galaxies throughout stellar population synthesis studies. In addition we take into account the gas content of both galaxies deriving the HI+He rotation curve. The deduced baryonic rotation curves (star+gas) are inadequate to account for the total mass of UGC 4284 and UGC 11861, for that reason we examine the possibility of dark matter to explain the incongruity between the observed HI and H α rotation curves of UGC 4284 and UGC 11861 and the derived baryonic rotation curves. We consider NFW, Burkert, DiCintio, Einasto, and the Stadel dark matter halos, to analyse the dark matter content of UGC 4284 and UGC 11861. The principal results of this work are that cored dark matter models better reproduce the dark matter H α and HI rotation curves of UGC 11861 and the dark matter HI rotation curve of UGC 4284, while, the H α rotation curve of UGC 4284 is better reproduced by a cuspy DiCintio DM model. In general, cored exponential two-parameters models Einasto and Stadel, give better fits than Burkert. This trend, as well as to confirm past results, presents for the first time a comparison between two different exponential dark matter models, Einasto and Stadel, in an attempt to better constrain the range of possible exponential dark matter models applied to real galaxies.

Key words: galaxies:irregular – galaxies:kinematics and dynamics – galaxies:individual:UGC 4284 – galaxies:individual:UGC 11861 – (cosmology:) dark matter

1 INTRODUCTION

The rotation of gas and/or stars in galaxies provides an important information about the kinematics of the galactic disk. Observed RCs are somewhat flat and no Keplerian decline was detected. The interpretation based on the dark matter (DM) paradigm assumes a large amount of DM far beyond the visible part of galaxies. Freeman (1970) was one of the first to suggest that RCs could be used as indication of DM, reporting that the RCs of NGC 300 and M33 did not show the expected Keplerian decline, and estimating that the DM mass in these galaxies should be at least as

large as the mass of the luminous matter. Rubin et al. (1980) and Bosma (1978, 1981a,b) endorse the evidence of DM, performing extensive studies of galaxies RCs in optical and radio wavelengths. Bahcall et al. (1982) built artificial RCs considering a central component, a disk, a spheroidal component and a DM component to determine unexpected deviations from the generally believed logarithmic slope of 2.0. Carignan & Freeman (1985) analysed the mass distribution of four galaxies detecting the necessity of a DM component to explain the observed RCs of those galaxies whose RCs extend to 1.5 – 3.0 R_{25} . These works turn out a general acceptance of the DM hypothesis.

In general, the first step to determine the DM distribution in galaxies is to recognize what kind (bulge, disk, and

* E-mail:prepetto@lna.br

bar) and how many stellar components constitute the innermost optical disk. This can be done by performing isophotal analysis on broad band image photometry of the studied objects. In fact, the luminosity profile obtained from galaxies observations, is the unique information to derive a coarse estimate of the visible mass of such objects, assuming a constant relation between luminosity (L) and mass (M). Once all the stellar components are identified, different mass profiles for the stellar disk, bulge, and bar are used to account for the stellar mass of the optical disk. The gas mass content is represented by the mass profile of the gaseous tracer (usually neutral hydrogen) used to measure the RC far from the optical disk extent. The DM halo is commonly considered spherically symmetric and its circular velocity is given by the ordinary Newtonian law. The next step is to accomplish a non-linear least squares fit to the observed RC considering a general fitting relation $V_{tot}^2(R) = [V_{\star}^2(R) + V_{gas}^2(R) + V_{halo}^2(R)]$. The problem arise for the luminous components, because in general the stellar mass is unknown and a guess of the mass-to-luminosity ratio (M/L) is required. In contrast, the gas amount is usually well-known and rather small (Swaters et al. 2000). During the fitting procedure, generally the M/L is a free and constant parameter given the ignorance about the stellar content of a disk galaxy.

The maximum disk hypothesis (MDH) was introduced by van Albada et al. (1985) and van Albada & Sancisi (1986) to study the DM distribution of NGC 3198 and it is based on the assumption that the DM halo dominates at radii greater than $2.2 R_D$. Inside this radius the luminous matter could account for the galaxy circular velocity estimated up to that radius. Ratnam & Salucci (2000) analysed the mass distribution of 83 spiral galaxies, using high resolution RCs data, formulated a more modern version of the MDH, suggesting a baryonic scale range in radius from $0.5 R_D \sim 0.5$ kpc to $2.0 R_D \sim 30.0$ kpc, where the luminous matter seems to produce a substantial part of the gravitational potential of the studied galaxies.

In general there are two main factors that govern the degeneracy of the results of the RCs fitting: actual errors in RCs measurements and our ignorance of the true distribution of luminous matter. Hypothetically, fitting different mass components to observed RCs should be a valid approach if we have a great number of high resolution data with negligible measurement errors. In practice the observed RCs are far from these ideal conditions, therefore the RCs decomposition continue to be a degenerate problem. A more robust determination of the distribution of the luminous matter based on more accurate constraints of the M/L variation with galactocentric radius and stellar colours could lessen the degree of degeneracy.

Some authors found a strong correlation between the variation of stellar M/L in optical and near-infrared (NIR) passbands and stellar population colours (Bell & de Jong 2001; Bell et al. 2003). Bell & de Jong (2001) also discovered that low luminosity galaxies have lower stellar M/L than high surface brightness galaxies and galaxies with few gas content. From these works it remains clear that to remove the above mentioned degeneracy, due to our poor knowledge of the stellar M/L , more information about the radial variation of the stellar M/L and the correlation with other galaxies properties are necessary. Gallazzi et al. (2005) ex-

plore the dependency among the total galaxy stellar mass, the stellar metallicity, and the stellar age, estimating these parameters for a magnitude-limited sample of $\sim 200,000$ galaxies selected from SDSS DR2. These authors made a comparison of the observed galaxy spectra and a large library of synthetic spectra based on Monte Carlo library of star formation histories (SFHs). Gallazzi et al. (2005) and Gallazzi et al. (2008) found a large scatter in the relations amidst stellar mass, age and metallicity, concluding that the physical parameters of galaxies at the present time are not uniquely determined by stellar masses, and that gas infall or outflow could also play an important role in building galactic physical properties.

From these works it is evident that the stellar M/L rely on so many physical parameters that the simplistic assumption of considering the stellar M/L constant along the galactic disk is unreal. In this respect, stellar population synthesis models (SPs) represent a valuable tool to constrain in a more realistic manner the true value of the stellar M/L . Zibetti et al. (2009) conceive a novel approach to build spatially resolved maps of stellar mass surface density considering broad-band photometry images of galaxies in the optical and NIR. The authors used a Monte Carlo library of 50,000 synthetic SPs by Bruzual & Charlot (2003) and Bruzual (2007) incorporating an updated recipe for the thermally pulsing asymptotic giant branch stellar evolutionary phase following Marigo & Girardi (2007) and Marigo et al. (2008). Gallazzi & Bell (2009) studied the accuracy in the determination of stellar M/L from galaxy colours, using the SPs models of Bruzual & Charlot (2003) and a Monte Carlo library of 150,000 SFHs, to examine which spectroscopic conditions and spectral signal-to-noise ratios (S/N) are required to decrease the errors on M/L determination for different galaxy types. The authors concluded that in galaxies with old stellar populations the accuracy of M/L is beneath 0.05 dex for $S/N > 20$, while for galaxies with young stellar population the M/L presents, in general, higher statistical uncertainties. The results of Gallazzi & Bell (2009) are based on the very strong assumption that the dust extinction is negligible. MacArthur (2005) prove that the effect of dust attenuation is important near 4000 \AA , additionally, from the literature it is well-known that dust effects have a crucial impact on M/L values based on colours (Zibetti et al. 2009). For this reason, at the moment, it does not exist a robust analysis discussing the feasibility of SPs studies to determine the M/L , nonetheless SPs seem to be the more powerful tool to obtain the stellar mass content of galaxies.

The Λ -CDM paradigm (Blumenthal et al. 1984) predicted cuspy DM density profiles in the centre of galaxies (Navarro et al. 1996) and recent results with higher resolution seem to suggest a shallower DM density profile (Navarro et al. 2004, 2010). Nonetheless the past and newer developments are in contradiction with observational results of cored DM density profiles in dwarf galaxies (de Blok et al. 2001; de Blok & Bosma 2002; Swaters et al. 2003; Chemin et al. 2011). This discrepancy is known as the cuspy-core problem. Many other authors, in an attempt to contribute to the solution of the cuspy-core problem, performed the RC decomposition considering a constant M/L (Carignan & Freeman 1985, 1988; Jobin & Carignan 1990; Persic & Salucci 1990; Martinbeau et al. 1994; Persic et al. 1996; Blais-Ouellette et al. 2001; de Blok et al. 2001; de Blok & Bosma 2002; Swaters et al. 2003;

Kuzio de Naray et al. 2006; Fuentes-Carrera et al. 2007; Spano et al. 2008; Kuzio de Naray et al. 2008; Repetto et al. 2010; Chemin et al. 2011) and reinforce the evidence of a cored DM distribution in the central part of galaxies. Conversely, other authors pursue spectrophotometric and SPs studies to derive the M/L of the stellar component (Salucci et al. 2008; Repetto et al. 2013; de Denus-Baillargeon et al. 2013) or at least to constrain the stellar component (Dutton et al. 2005) to avoid the disk-halo degeneracy. Salucci et al. (2008) accomplished RCs mass modelling and spectral energy distribution fitting with spectrophotometric models to obtain the disk masses of 18 Sa spiral galaxies (principally bulgeless systems) finding that by decomposing the RCs with the spectrophotometric disk masses the results are consistent with the corresponding maximum disk solution. Repetto et al. (2013) employed the Zibetti et al. (2009) method to optical (SDSS) and NIR (2MASS) images of NGC 5278 (KPG 390A) to obtain the stellar disk mass profile of that galaxy from SPs models to reproduce the RC of KPG 390A. The new strategy relied on fitting only the DM RC, obtained by subtracting the SPs baryonic disk from the observed RC of NGC 5278. The most important finding of Repetto et al. (2013) is that the favoured DM distribution is cored when the disk mass approximate to the maximum disk solution in agreement with the general belief. de Denus-Baillargeon et al. (2013) used a chemo-spectrophotometric galactic evolution model to determine the stellar M/L and perform the RC decomposition of ten spiral and dwarf irregular galaxies from the SINGS survey (Kennicutt et al. 2003). The authors employed the settled baryonic disk as a weighting function to fit the model DM halo to the RCs of the studied subsample of galaxies, and concluded that the stellar disks obtained from their chemo-spectrophotometric models were compatible with the maximum disk hypothesis. The few examples presented, indicate that a growing effort to break the disk-halo degeneracy exists, however the most significant contributions trying to address the cuspy-core problem still rely on the general assumption of considering the stellar M/L constant along the galactic disk. In general, it is still missing a significant endeavour to earn the DM distribution, through RC fitting, determining the disk stellar mass from SPs studies. For this reason it is worth considering the cuspy-core problem with a different observational approach, focusing on the formulation of a general procedure to better constrain the baryonic disk mass in galaxies. This is the first of a series of papers dedicated to the study of the outer and inner mass distribution in irregular galaxies, applying and testing the novel method of Repetto et al. (2013), using the RCs data of the WHISP HI survey of galaxies (Verheijen & Sancisi 2001), to investigate the outer mass distribution, and the GHASP H α survey of galaxies, to analyse the inner mass distribution (Amram et al. 2002; Garrido et al. 2002; Spano et al. 2008; Epinat et al. 2008). In this first article we concentrate on the determination of the mass distribution of two irregular galaxies UGC 4284 and UGC 11861, whose RCs are somewhat symmetric and regular and for this reason more suitable to perform the RC analysis. The novelty of the approach conceived in Repetto et al. (2013) resides in deriving the stellar disk mass of the galaxy from SPs studies and in subtracting the built baryonic disk from the observed RC to fit only the remaining DM RC as we have already summarised above.

The main motivation of these works are attempt to answer the following question: Performing the RC decomposition with more realistic M/L obtained from SPs studies, could change the determination of the DM halo parameters substantially? In the case of a positive answer, this research could shed new light on how the DM halo parameters change because of a non parametric baryonic component. In the case of a negative answer the analysis is still worth to characterise a novel procedure to constrain the stellar disk parameters with a deeper knowledge of the physics of the underlying stellar disk populations derived from photometric data.

This paper is organized as follows. Sections 2 and 3 describe the GALFIT disk/bulge/bar decomposition. Section 4 describes the constraints of the baryonic M/L ratio through SPs. Section 5 describes the H α and HI RC derivations. Section 6 presents the analysis of the inner and outer DM distributions. Section 7 discusses the results. Finally, Section 8 presents our conclusions.

2 2D GALFIT DISK/BULGE/BAR DECOMPOSITION OF UGC 4284

UGC 4284 is classified as Scd(s) in the RC3 (de Vaucouleurs et al. 1991), and as SABc by Paturel et al. (2003). Kandalian & Kalloghlian (1998), Chapelon et al. (1999) and Cabrera-Lavers & Garzón (2004) found evidence of a central isophotal distortion that they explain postulating the existence of a bar with diameter of 38". Other authors did not confirm the presence of a bar in UGC 4284, nevertheless they encountered non-circular and off-plane gas motion in the inner region of UGC 4284 that they discuss as originated by a warped gaseous disk (Coccatto et al. 2004; Józsa 2007). Bearing in mind the purpose of the present study it is important to determine which kind of baryonic components do actually exist for UGC 4284, and given the incongruity of the above reported results we required to perform 2D isophotal analysis of the surface brightness of this galaxy, using GALFIT (Peng et al. 2002, 2010) and considering at least three principal components: disk, bulge and bar. UGC 4284 has been observed with Hubble Space Telescope (HST) in the filters F555W (WFPC2 V), F814W (WFPC2 wide I) and F606W (WFPC2 wide V), nonetheless the filters F555W and F814W show only a small part of the periphery of the galaxy. In contrast the filter F606W exhibits a larger portion of the disk of UGC 4284, so we use that filter to decompose the disk of UGC 4284. The results of the 2D exponential disk fit are presented in Table 1. In the case of UGC 4284 we also examined the possibility of a bulge and a bar components given the inconsistency in the morphological classification of this galaxy. We use the Spitzer IRAC 4.5 μ m image because UGC 4284 is indiscernible in the 2MASS J, H, K bands, and in all the SDSS filters is too faint to allow an obvious separation from the background. Neither the Sersic component nor the Ferrers (Ferrers 1877) component produce acceptable fit parameters to reveal the presence of a bulge and a bar, for this reason we conclude that UGC 4284 has only an exponential disk component in total agreement with the RC3 classification.

Table 1. Results of GALFIT isophotal analysis for UGC 4284.

UGC 4284 exponential disk final parameters.	
Surface Brightness (mag arcsec ⁻²)	17.97
Scale length (kpc)	1.27
Axial ratio	0.46
Inclination (degrees)	64.98
Position Angle (degrees)	44.45

3 2D GALFIT DISK/BULGE/BAR DECOMPOSITION OF UGC 11861

UGC 11861 was classified as SABdm in the RC3 (de Vaucouleurs et al. 1991), as SABd by Paturel et al. (2003). At first glance the presence of a bar is not so evident from single optical (SDSS) and NIR (2MASS) broad band images, nevertheless a central boxy structure is clearly visible in the Spitzer IRAC 3.6 μ m image. The congruity in the morphological taxonomy of UGC 11861 allow us to identify promptly at least two components for that galaxy: a disk and a bar. We use GALFIT to prove the existence of such structures for UGC 11861. We employ the SDSS g band image for the disk and the Spitzer IRAC 3.6 μ m image for the bar. We consider an exponential disk and Ferrers model (Ferrers 1877) for the bar. The GALFIT result for the disk and bar GALFIT model are listed in Table 2. We also consider the possibility of a bulge component for UGC 11861, for which we adopt a Sersic profile and we fit with GALFIT 2MASS J, H, and K band images regarding a de Vaucouleurs bulge with an older stellar population, and SDSS g,r and i band images considering the possible presence of pseudobulges with younger stellar population. The choice of that photometric range to examine the possible existence of a bulge for UGC 11861 is also dictated by the fact that the bar emission is fainter in the selected passbands, and this fact could in principle allow an unambiguous detection of a potential bulge. In the case of the SDSS g, r and i bands we first fit an exponential disk model and then we try to fit a Sersic component to detect the existence of an hypothetical bulge in the residuals without success. The GALFIT fit to the 2MASS J, H, and K passbands did not reveal the presence of a bulge. From the GALFIT analysis we conclude that UGC 11861 is composed of an exponential disk and a bar, in good agreement with the morphological classification of that galaxy.

4 BARYONIC M/L RATIO FROM RESOLVED MASS MAPS

Reliable M/L ratios are an important aspect when determining the baryonic contribution to the rotation curves of disk galaxies. By using a chemo-spectrophotometric galactic evolution model de Denus-Baillargeon et al. (2013) highlighted the importance of adopting a radially varying M/L ratio, vs. a radially constant one (see also Repetto et al. 2013).

In this work we adopt a resolved mass map method (Zibetti et al. 2009) that relies on a Monte Carlo library

Table 2. Results of GALFIT isophotal analysis for UGC 11861.

UGC 11861 exponential disk final parameters.	
Surface Brightness (mag arcsec ⁻²)	19.35
Scale length (kpc)	1.30
Axial ratio	0.47
Inclination (degrees)	64.27
Position Angle (degrees)	71.46
UGC 11861 Ferrers bar final parameters.	
Surface Brightness (mag arcsec ⁻²)	8.83
Outer truncation radius (kpc)	2.48
α	2.95
β	0.0
Axial ratio	0.38
Inclination (degrees)	70.74
Position Angle (degrees)	-16.6

of 50,000 stellar population spectra randomly drawn from the SPS models of S. Charlot & G. Bruzual (CB07). These models use single stellar populations as described by Bruzual & Charlot (2003), but include the prescription for stellar evolution in the thermally-pulsating asymptotic giant branch (TP-AGB) by Marigo & Girardi (2007). The IMF of Chabrier (Galaxy-disk, 2003) is adopted. The adjustable parameters of the models are the star formation history (SFH), which is exponentially declining with random bursts superimposed, the metallicity, uniformly distributed between 0.02 and 2 times solar, and the extinction by dust, based on the two-component model of Charlot & Fall (2000).¹ The Monte Carlo library is obtained for a given combination of colours, and the mass-to-light ratio (M/L) for a given filter.

Zibetti et al. (2009) fiducial method involves the use of the g and i bands from SDSS, and one NIR filter. The main reason for the use of this combination of filters is that it provides the less degeneracy for the SPs models in a colour-colour diagram (e.g., $g - i$, vs. $i - H$). Other combinations of filters, e.g. Johnson's V and I combined with one NIR filter, show a smaller area in the colour-colour diagrams, thus providing more degeneracy, i.e., the same colours can be attributed to many different model parameters. The same applies to various other combinations of filters (see figure 1). It was found that the absolute mass values are overestimated, as compared to the fiducial method, when a combination of colours with more degeneracy is adopted.

The M/L is obtained for the NIR filter as a function of $(g - i)$ and, e.g., $(i - H)$. The models are grouped in bins that take into account the observational error in the photometry, typically 0.05 mag. For each bin, the median value of M/L is computed. The final look-up tables can be compared with observations in a pixel-by-pixel basis. A map of M/L is obtained which can be converted to absolute mass if the distance to the object is known.

When analysing the spectral energy distribution (SED) of galaxies, the wavelength range between 2.5 μ m and 10 μ m

¹ The model takes into account the fact that stars are born in dense molecular clouds. A different treatment is given for the attenuations of young and old stars.

is considered to be a mixture of stellar and dust emission (e.g., da Cunha et al. 2008). In order to apply the resolved mass map method (Zibetti et al. 2009) to get a M/L map of, e.g., the IRAC 3.6 μ m filter, an infrared SED model is needed. The model of da Cunha et al. (2008) is adequate for this purpose. This model incorporates four main dust components, the emission from polycyclic aromatic hydrocarbons (PAHs), the mid-IR continuum from hot dust, and both the emission from warm and cold dust in thermal equilibrium. An energy balance condition is applied in a way that the total energy absorbed by dust, in stellar birth clouds and in the diffuse ISM, is re-radiated in wavelengths over the range from 3 μ m to 1000 μ m. It is assumed that the dust in the ISM is heated only by starlight. The infrared model can be easily combined with the SPs models of Bruzual & Charlot (2003) and CB07. A Monte Carlo library of 50,000 dust emission spectra, for wide ranges of dust temperatures and fractional contributions by the different dust components, is provided in the MAGPHYS² package of da Cunha et al. (2008). We combine this library with the SPs library taking care of the energy balance condition as described in da Cunha et al. (2008). A total of 667 million spectra were obtained. The models were grouped in bins of $0.05 \times 0.05 \text{ mag}^2$, for the $(g-i)$, and $(i-3.6\mu\text{m})$ colours. The mean M/L ratio for the 3.6 μ m filter was obtained for each bin. The results are shown in figure 2, together with the rms values.

We then use these results (in figure 2) to obtain the two-dimensional stellar mass map, for UGC 11861. In figure 3 we show the azimuthally-averaged radial profiles of the $M/L_{(3.6\mu\text{m})}$ ratio (left plot), and the stellar (μ_*) mass surface density (right plot). We assume an object distance of 18.4 Mpc, and correct the models for Galactic extinction (Schlafly & Finkbeiner 2011; Chapman et al. 2009).

For the case of UGC 4284 the resolved mass map method was also adopted. The 3.6 μ m data was taken from the Spitzer Survey of Stellar Structures in galaxies (Sheth et al. 2010). The resulting azimuthally averaged radial profiles for the $M/L_{3.6\mu\text{m}}$ ratio, and the stellar mass surface density (μ_*) are shown in figure 4. We assume a distance of 9.42 Mpc.

4.1 Baryonic HI+He gas components of UGC 4284 and UGC 11861

The HI gaseous RCs of both galaxies were obtained integrating the total HI column density map in elliptical rings using the task *ELLINT* in the *GIPSY* package. The outputs are the HI mass surface density and the HI cumulative mass displayed in figures 5 and 6. The contribution of He and metals was taken into account scaling by a factor of 1.4 the HI surface density and mass. The total HI+He RCs of both galaxies are displayed in figure 7.

5 H α AND HI RC OF UGC 4284 AND UGC 11861

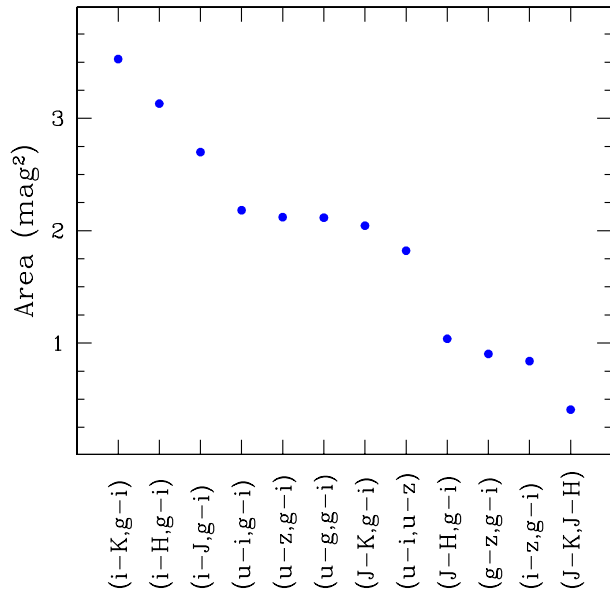


Figure 1. Area covered in a colour-colour diagram, for different colour combinations obtained from a Monte Carlo SPs library grouped in colour bins of $0.05 \times 0.05 \text{ mag}^2$, as described in Zibetti et al. (2009). Filters u , g , i , and z from SDSS. Filters J , H , and K from 2MASS.

The H α RCs of UGC 4284 and UGC 11861 were derived in the frame of the Gassendi H α survey of spirals (GHASP Garrido et al. 2002), dedicated to study the 2D H α velocity field and RCs of a sample of 203 spiral and irregular galaxies. Garrido et al. (2003, 2004, 2005) perform the first data reduction and analysis of 97 galaxies in the GHASP sample. Epinat et al. (2008) accomplished again the reduction process of the 97 galaxies more 108 new galaxies, using adaptive binning technique based on Voronoi tessellation in order to provide different weights for low and high signal-to-noise zones in the velocity fields. The final high resolution 2D velocity fields of the GHASP survey have a spectral accuracy of about 5 km s^{-1} and a spatial resolution of $\sim 2''$. From those high resolution 2D velocity fields, Epinat et al. (2008) constructed the RCs for the most galaxies of that survey. A part of the GHASP sample (130 galaxies) has been previously observed by the Westerbork survey of HI in spiral galaxies (WHISP) intended to investigate the 2D HI kinematic of 500 spiral and irregular galaxies (Verheijen & Sancisi 2001). The typical spectral resolution of the WHISP sample of 2D HI velocity fields is about 5 km s^{-1} with a spatial resolution of $\sim 12''$.

van Eymeren et al. (2011) obtained the HI RCs of a sample of 70 spiral and irregular galaxies, also including UGC 4284 and UGC 11861, using the WHISP HI velocity fields by applying a tilted-ring analysis to derive accurately the kinematic parameters from the velocity fields, obtaining residuals of a few km s^{-1} . In the particular case of UGC 4284 and UGC 11861, the HI WHISP RCs are relatively more extended than the H α RCs, they are regular and in the inner regions they have a good accordance with the H α RC. We decide to use the H α RCs to explore the inner DM distribution and the HI RCs to study the outer

² <http://www.iap.fr/magphys/magphys/MAGPHYS.html>

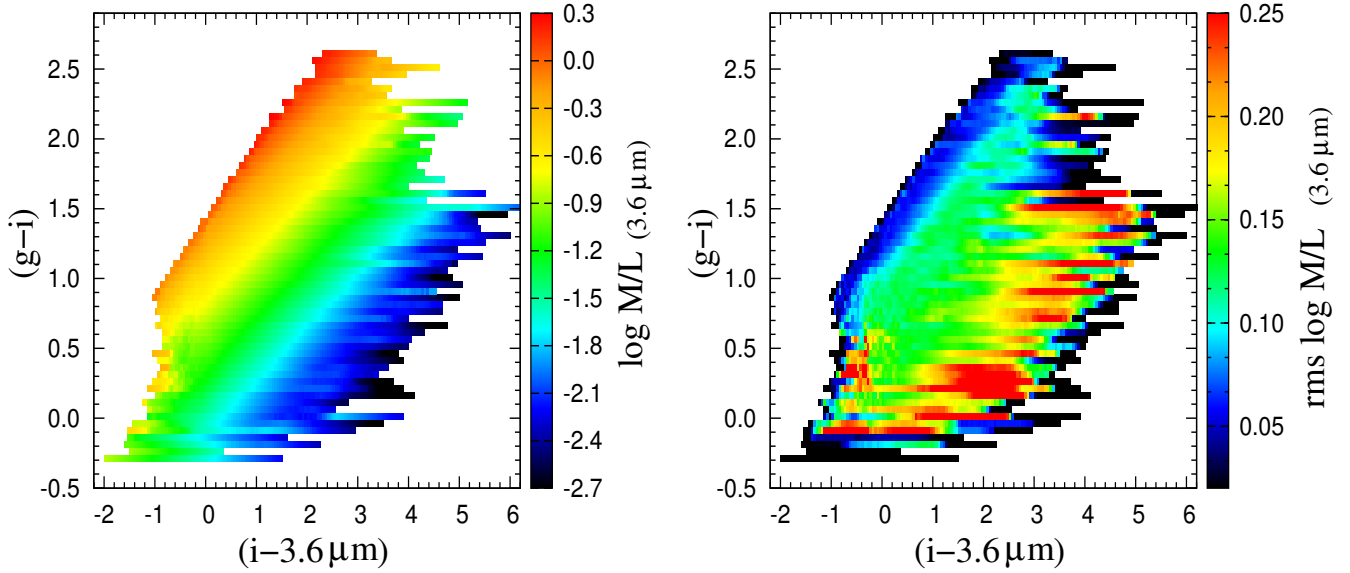


Figure 2. *Left:* Logarithm of the effective, i.e., as seen by the observer, M/L ratio for the $3.6\mu\text{m}$ filter, $M/L_{(3.6\mu\text{m})}$, in a $(g-i)$, vs., $(i-3.6\mu\text{m})$, colour-colour diagram. Data are grouped in bins of $0.05 \times 0.05 \text{ mag}^2$. *Right:* Logarithm of the root mean square (rms) errors, corresponding to the $M/L_{(3.6\mu\text{m})}$ data in the left panel. The mean error value (of all plotted data) is $\sim 30\%$.

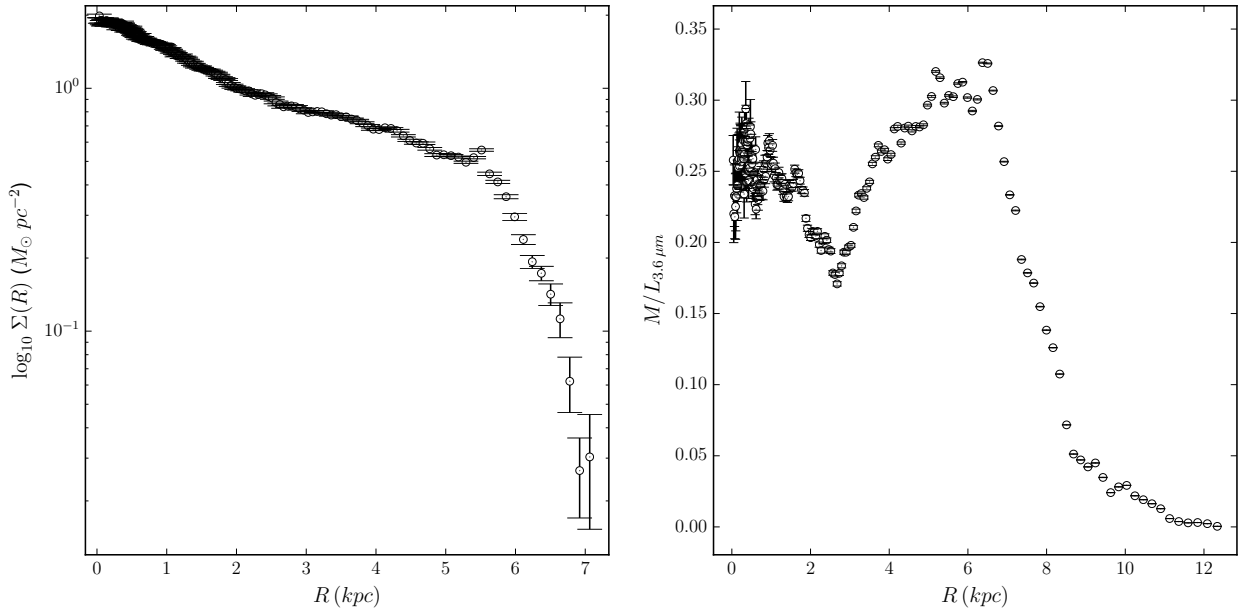


Figure 3. Radial profiles for UGC 4284. *Left:* Azimuthal average of the stellar mass surface density, μ_* , as a function of radius. *Right:* Azimuthal average of the mass-to-light ratio, $M/L_{3.6\mu\text{m}}$, as a function of radius. An inclination angle of 59° , and position angle of 169.9° , were adopted as deprojection parameters.

DM distribution. The comparison between the $\text{H}\alpha$ and HI RCs is shown in figure 7. In the same figure are also presented the baryonic RCs, considering errors giving a variation of more and less 30% of the disk mass for both galaxies. From figure 7 it is clear that stars and gas alone are not enough to account for the total mass of UGC 4284

and UGC 11861. The total disk mass of UGC 4284 is $M_d = 7.92 \times 10^9 M_\odot$, the total disk mass of UGC 4284 more 30% is $M_d = 1.03 \times 10^{10} M_\odot$ and the total disk mass of UGC 4284 less 30% is $M_d = 5.55 \times 10^9 M_\odot$. The total disk mass of UGC 11861 is $M_d = 5.38 \times 10^{10} M_\odot$, the total disk mass of UGC 11861 more 30% is $M_d = 6.99 \times 10^{10} M_\odot$ and the total

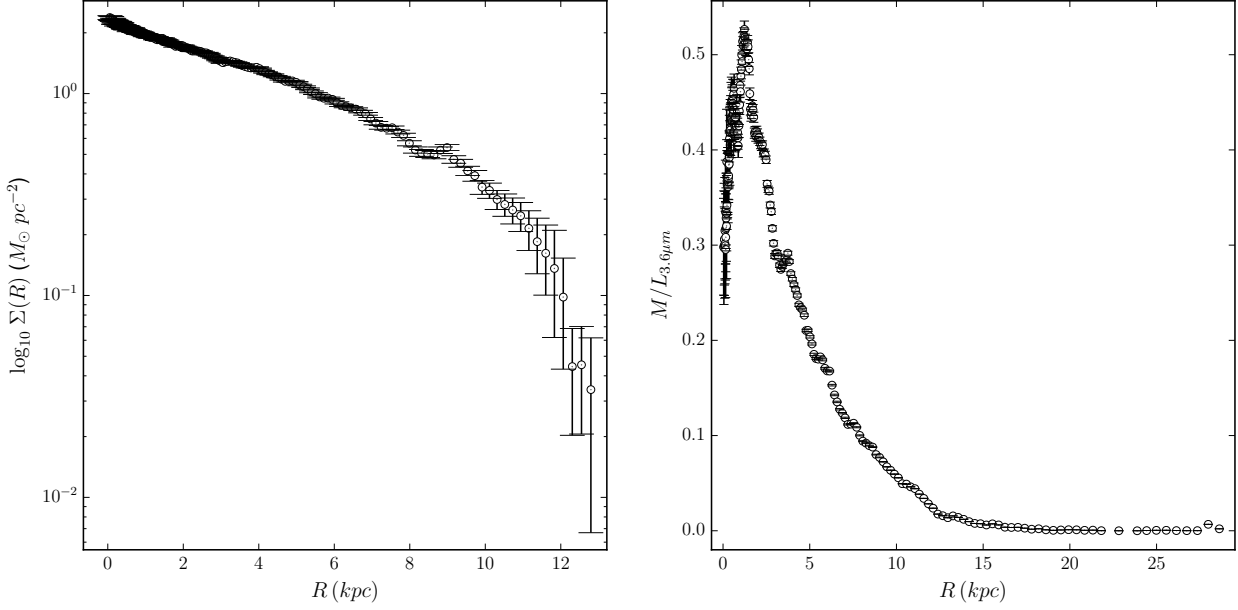


Figure 4. Radial profiles for UGC 11861. *Left:* Azimuthal average of the stellar mass surface density, μ_* , as a function of radius. *Right:* Azimuthal average of the mass-to-light ratio, $M/L_{(3.6\mu m)}$, as a function of radius. An inclination angle of 61° , and position angle of 10.7° , were adopted as deprojection parameters.

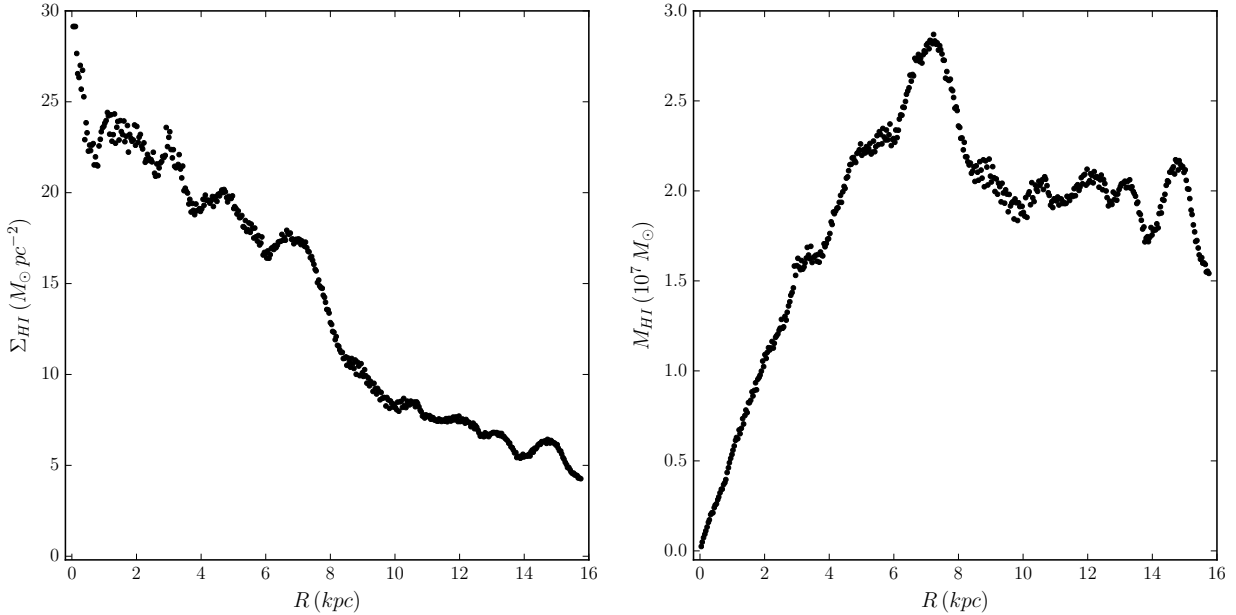


Figure 5. HI mass gas profiles for UGC 4284. *Left:* Azimuthal average of the HI mass surface density, Σ_{HI} , as a function of radius. *Right:* Azimuthal average of the HI mass, M_{HI} ($10^7 M_\odot$), as a function of radius. An inclination angle of 59° , and position angle of 169.9° , were adopted as deprojection parameters.

disk mass of UGC 11861 less 30% is $M_d = 3.76 \times 10^{10} M_\odot$. In the case of UGC 11861 the disk mass is the sum of the disk and the bar component (see section 3). In the next two sections we explore the possibility of DM, for UGC 4284 and UGC 11861, to explain the discrepancy between the to-

tal observed mass distribution and the mass content due to stars and gas.

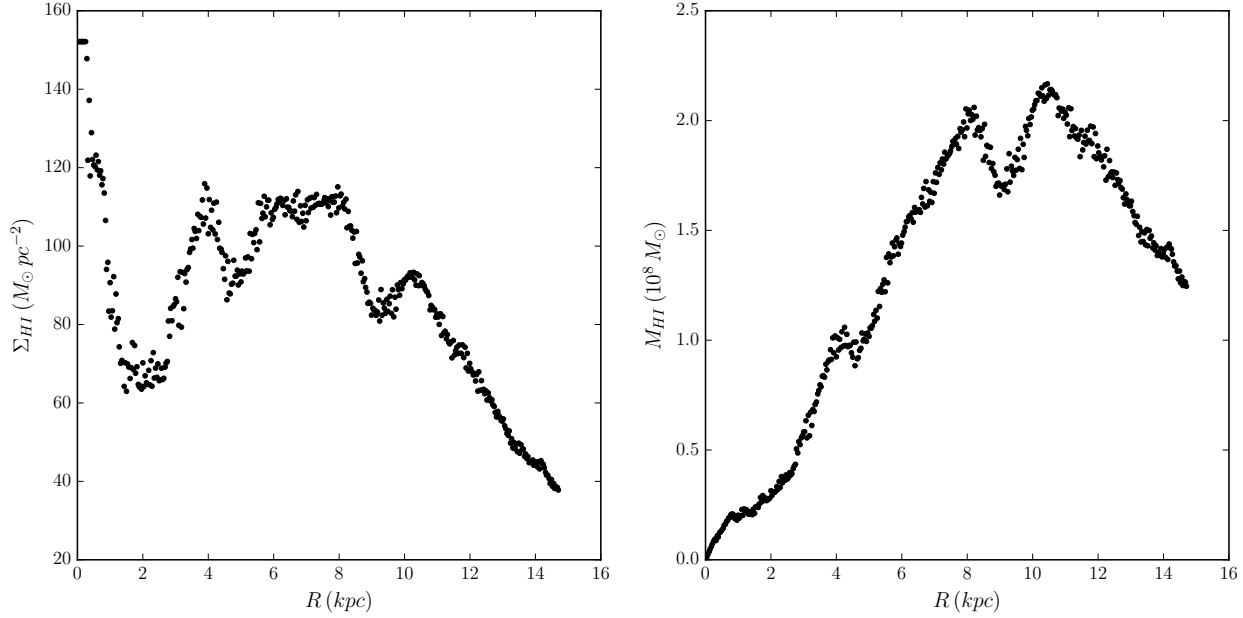


Figure 6. HI mass gas profiles for UGC 11861. *Left:* Azimuthal average of the HI mass surface density, Σ_{HI} , as a function of radius. *Right:* Azimuthal average of the HI mass, M_{HI} ($10^8 M_{\odot}$), as a function of radius. An inclination angle of 61° , and position angle of 10.7° , were adopted as deprojection parameters.

6 INNER AND OUTER DM DISTRIBUTION FOR UGC 4284 AND UGC 11861

We investigate the inner and outer DM content of UGC 4284 and UGC 11861 accomplishing the $H\alpha$ and the HI DM RCs fitting for both galaxies, considering possible errors in the stellar disk determination of plus and minus 30% for all the DM models examined in this study. The HI DM RCs were derived by subtracting the stellar RCs and also the HI+He gaseous RCs from the observed HI RCs of both galaxies.

We consider the DM halo of Navarro et al. (1996) (NFW), the Burkert (BK) Burkert (1995) DM halo and the Di Cintio et al. (2014) DM halo (DC). The DC DM halo was formulated from the double power-law model of Zhao (1996) expressing the three power-law exponents as functional forms of the stellar-to-halo mass ratio, establishing a two free parameters DM halo. We use the prescription of Dutton & Macciò (2014) for the concentration parameter for the NFW DM halo.

In the present study we use the *minuit* minimizer through the ROOT package written in C++. The ROOT package is a huge object-oriented data analysis framework developed at CERN that allows sophisticated analysis of practically any kind of data. The *minuit* minimizer uses the MIGRAD algorithm that implements a variable metric method, with inexact line search checking for positive-definiteness. The main difference with respect to the Levenberg-Marquardt method is that, the minimization algorithm only converges on the global minimum, for this purpose an important output parameter is the estimated distance from the (global) minimum (Edm), a quantity that informs the user when the global minimum is reached. The

Edm together with the χ^2 values and also the χ^2 filled contours, represent the fundamental criteria used in this study to assess the reliance of the determined solutions.

The fitting procedure employed in this study considers as free parameters the DM halos masses and radii respectively within the intervals $[10^8, 10^{14}] M_{\odot}$ and $[0.1, 100.0]$ kpc. The solutions we have found are listed in tables 2, 3, 4 and 5. In addition, the results with stellar disk mass $M_d = 7.92 \times 10^9 M_{\odot}$ for UGC 4284 and stellar disk mass $M_d = 5.38 \times 10^{10} M_{\odot}$ for UGC 11861 are displayed in figures 8-13. The χ^2 filled contours of the solutions presented in figures 8 to 13 are exhibited in figures 14 and 15.

From the tables and figures presented in this section it is evident that the NFW DM halo does not fit either the $H\alpha$ or the HI DM RCs of UGC 4284 and UGC 11861. The Edm indicates that the solution is far from the expected global minimum and this fact is also confirmed by the non existence of the χ^2 filled contours. The BK DM halo fits the $H\alpha$ and HI DM RCs of UGC 4284 and UGC 11861 better than NFW, even if the χ^2 filled contours are narrow and for the HI DM RC of UGC 4284 the final halo mass value coincide with the lower halo mass limit allowed by our fitting procedure.

The DC DM halo seems to perform better than BK DM halo as indicated by the χ^2 values, the χ^2 filled contours and the Edm values, even if in the case of the DM RC of UGC 11861 the χ^2 values for the BK DM halo are lower than the DC DM halo. The DM masses originated from the fitting of the DC DM halo are in general a factor $10^2 - 10^3$ times greater than the DM halo masses generated by the fitting of the BK DM halo. In the case of the HI DM RC of UGC 11861 the DM masses of the DC DM halo are a factor of 10^4 greater than BK DM halo, even if in this case the BK DM

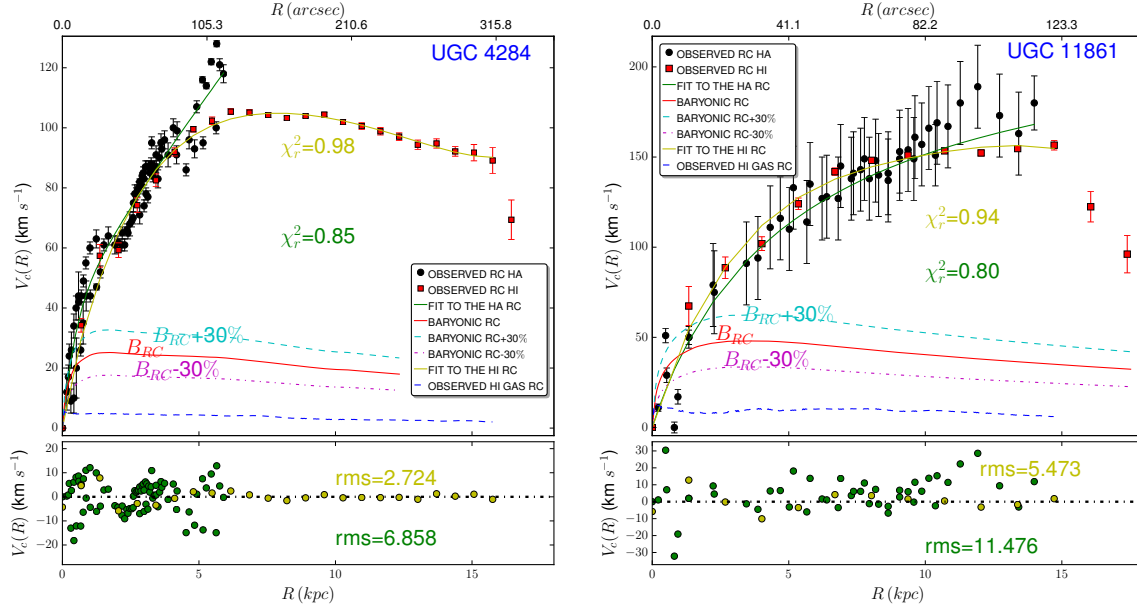


Figure 7. H α and HI RCs of UGC 4284 and UGC 11861 together with the corresponding baryonic stellar and gaseous (HI+He) RCs. The comparison between the two tracers is to motivate our choice to use the H α RCs to analyse the inner DM distribution and the HI RCs to estimate the outer DM distribution. In this figure is also shown the preliminary fit to the H α and HI RCs with the corresponding χ^2 values and residuals. The functional forms used for the preliminary fit are exponential-like for the H α RCs of UGC 4284 and UGC 11861 and polynomials for the HI RCs of both galaxies. We used those preliminary fits instead of the observed H α and HI RCs to perform the subsequent analysis.

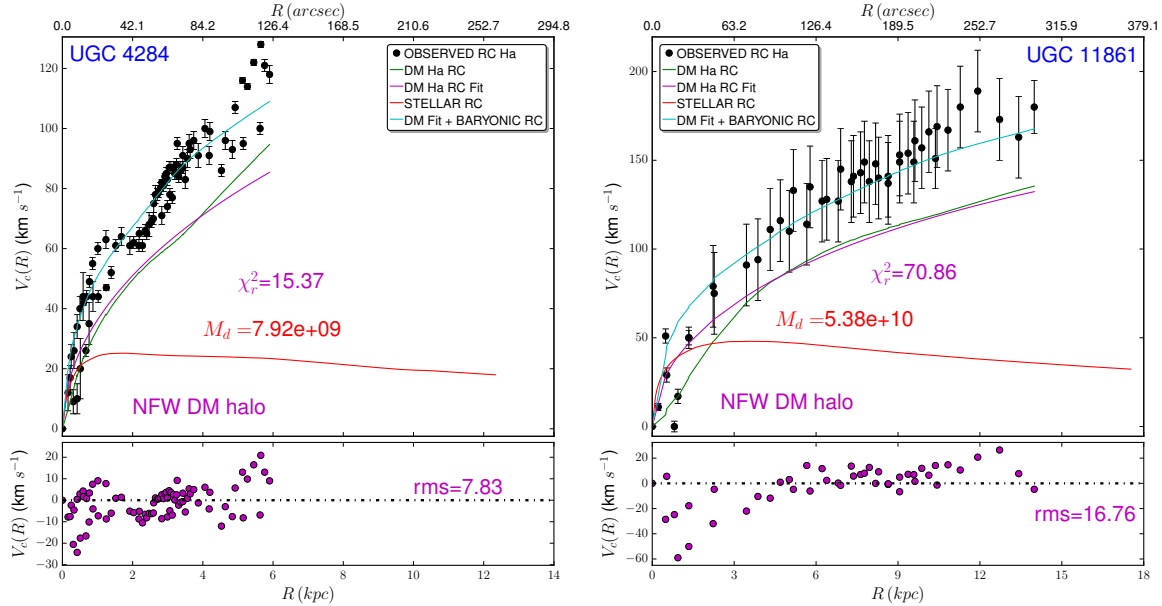


Figure 8. Left: NFW fit of H α DM RC of UGC 4284. Right: NFW fit of H α DM RC of UGC 11861. In both cases the χ^2 contours contain less than four points. For this reason we do not show that information for these solutions. The number of degrees of freedom (DOF) are 78 for UGC 4284 and 43 for UGC 11861.

halo accomplish better than the DC DM halo. Considering the range of disk stellar masses analysed in this study (see section 5) and DM halo masses obtained throughout this analysis for the DC DM halo our results reproduced closely the results presented by Di Cintio et al. (2014) (see figure 4 of the quoted article), in fact the inner slope outcome from

the DM RC fitted in this work with the DC DM halo are inside the interval $[-0.6, -1.2]$, therefore the results of the fits performed with the DC DM halos give in all cases a cuspy DM profile. This fact could in part justify the higher DM halo masses, with respect to BK DM halo, needed to reproduce the DM RCs considered in this work using the

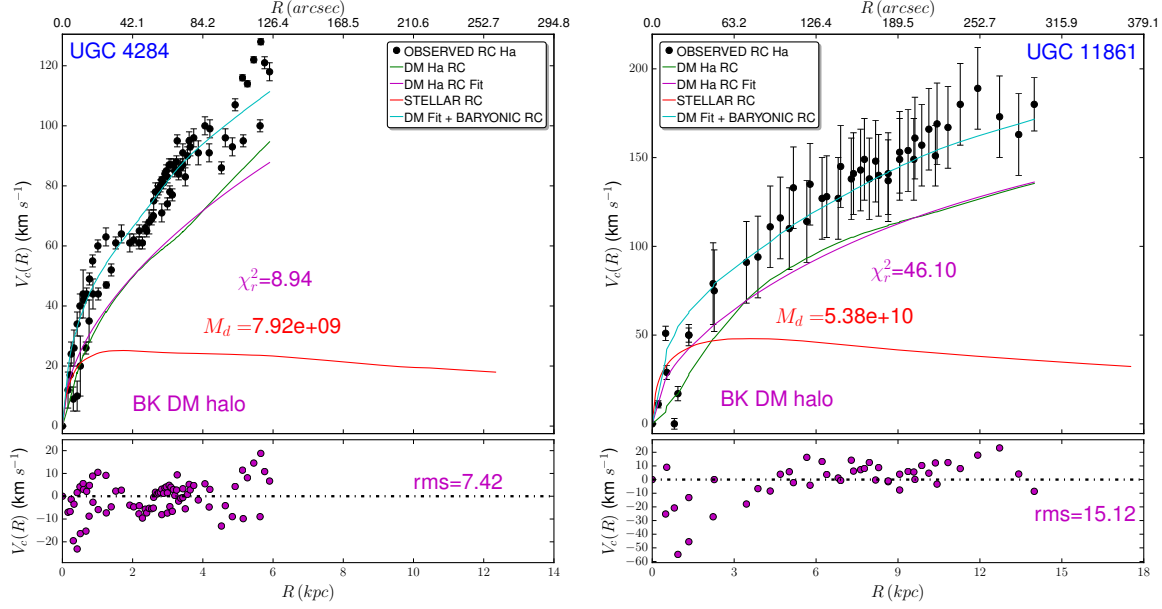


Figure 9. Left: BKH fit of H α DM RC of UGC 4284. Right: BKH fit of H α DM RC of UGC 11861. The number of degrees of freedom (DOF) are 78 for UGC 4284 and 43 for UGC 11861. The χ^2 contours are displayed in figure 14.

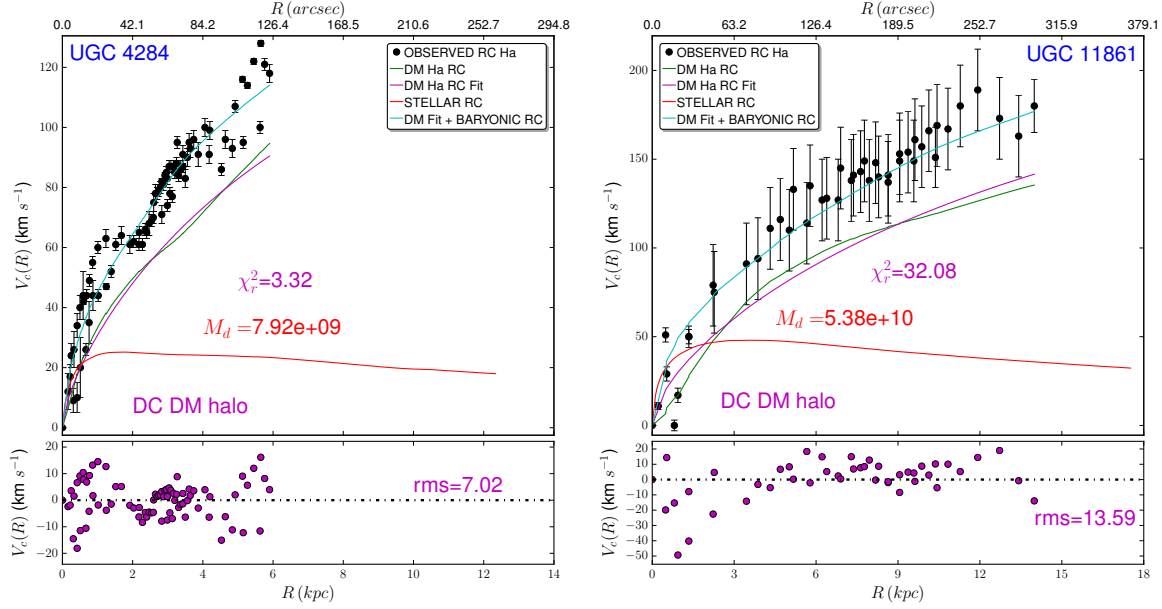


Figure 10. Left: DCH fit of H α DM RC of UGC 4284. Right: DCH fit of H α DM RC of UGC 11861. The number of degrees of freedom (DOF) are 78 for UGC 4284 and 43 for UGC 11861, the corresponding contours are displayed in figure 15.

DC DM halo. In general the fitting errors are about 0.01% for the DM halos radii and 0.1% for the DM halos masses, in the case where the DM halos fits succeeded.

In Appendix A we additionally test the Einasto (Einasto 1965) DM halo (HE) and the Stadel (Stadel et al. 2009) DM halo (HSD) as feasible options to model the H α and HI DM RCs of UGC 4284 and UGC 11861. Our purpose is to compare the outcome from these two DM halos with the other results encountered in this research to establish if the analysed RCs are best reproduced by cuspy or core profiles. As mentioned in Appendix A we regarded the HE and

HSD DM halos as two free parameters DM halos fixing the third parameters for both halos in order to have the same degrees of freedom of the other DM halos considered in this work. The results showed in the tables A1 and A2 clearly determine that the cored HE and HSD DM halos fits better than BK DM halo and also than DC DM halo practically in all cases, with the exception of the DM H α RC of UGC 4284 where the DC DM halo produces better results. In summary our main result is that the cored DM profiles HE and HSD better represent the DM content of UGC 4284 and UGC 11861.

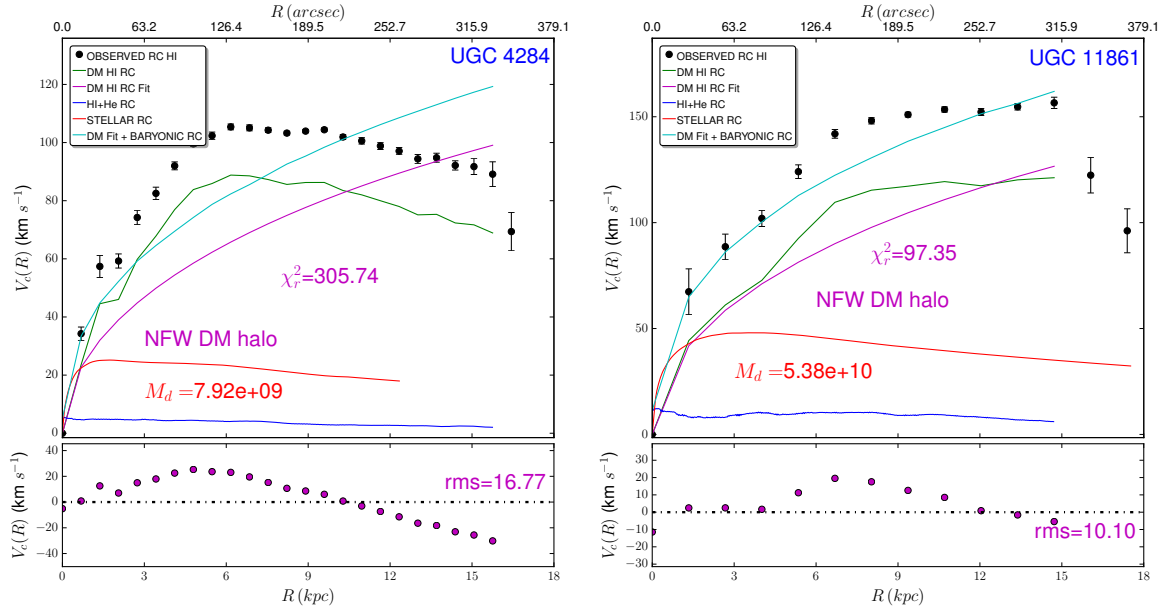


Figure 11. Left: NFW fit of HI DM RC of UGC 4284. Right: NFW fit of HI DM RC of UGC 11861. In both cases the χ^2 contours contain less than four points for this reason we do not show that information for these solutions. The number of degrees of freedom (DOF) are 22 for UGC 4284 and 10 for UGC 11861.

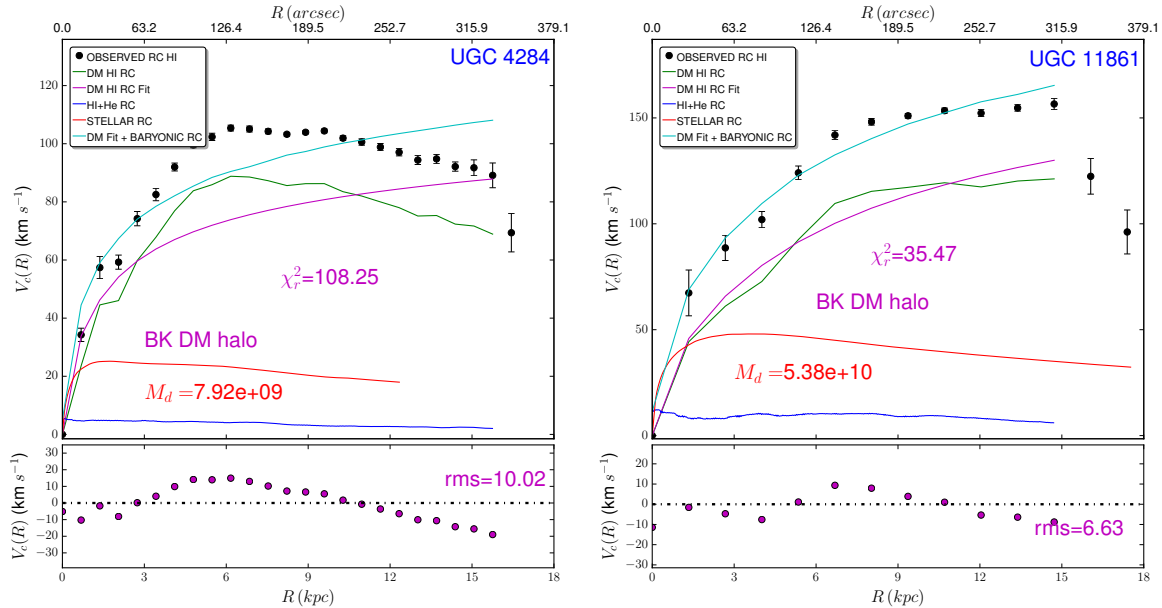


Figure 12. Left: BKH fit of HI DM RC of UGC 4284. Right: BKH fit of HI DM RC of UGC 11861. The number of degrees of freedom (DOF) are 22 for UGC 4284 and 10 for UGC 11861. The χ^2 contours are displayed in figure 14.

7 DISCUSSION

The Λ CDM (Λ Cold Dark Matter) paradigm, predicts cuspy density DM profiles in the centre of galaxies, whereas observational tests, using RCs analysis of spirals, irregular, dwarf, and low surface brightness galaxies found that cored density DM profiles better represent the central part of observed galaxies. The disagreement between the Λ CDM scenario and the observational results, led to consider possible modifications to the Λ CDM scheme. One possible refinement of the Λ CDM paradigm consists on the incorporation of bary-

onic physics on small scales (< 1 kpc). The basic idea to transform a cuspy central density profile to a cored one, is to remove baryonic matter from the central kpc of galaxies through some perturbation to their gravitational potential. Supernova explosions and driven-gas outflows, for instance, could be very efficient processes to obtain a central DM core in the centre of galaxies. Other possible mechanisms are gas and metals cooling and star formation. Some numerical and analytical attempts have been successful to achieve the de-

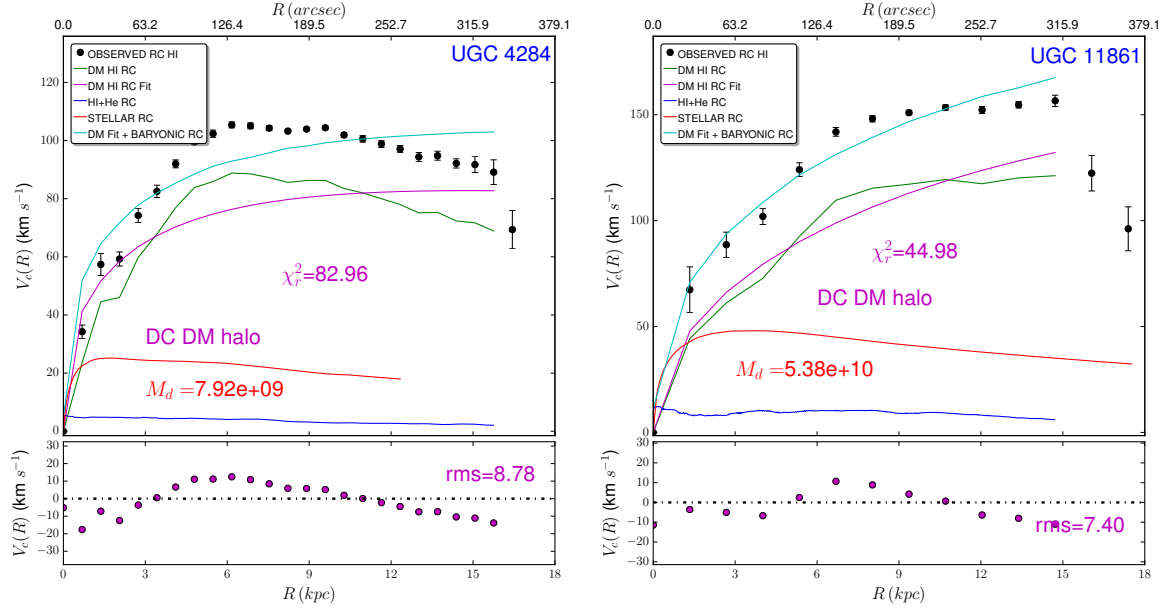


Figure 13. *Left:* DCH fit of HI DM RC of UGC 4284. *Right:* DCH fit of HI DM RC of UGC 11861. The number of degrees of freedom (DOF) are 22 for UGC 4284 and 10 for UGC 11861. The χ^2 contours are displayed in figure 15.

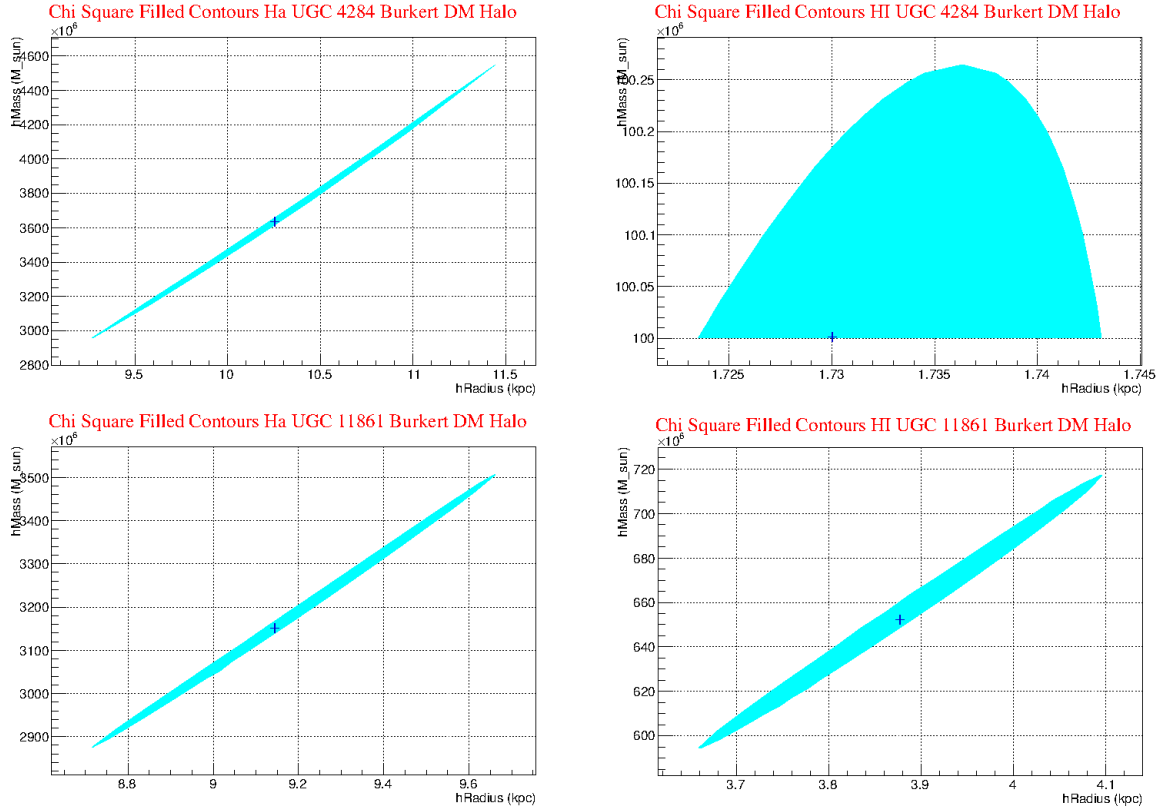


Figure 14. χ^2 filled contours at 70% confidence level. *First Panel:* H α DM RC of UGC 4284 BKH fit. *Second Panel:* HI DM RC of UGC 4284 BKH fit. *Third Panel:* H α DM RC of UGC 11861 BKH fit. *Fourth Panel:* HI DM RC of UGC 11861 BKH fit. The blue crosses represent the solutions found through the fitting procedure.

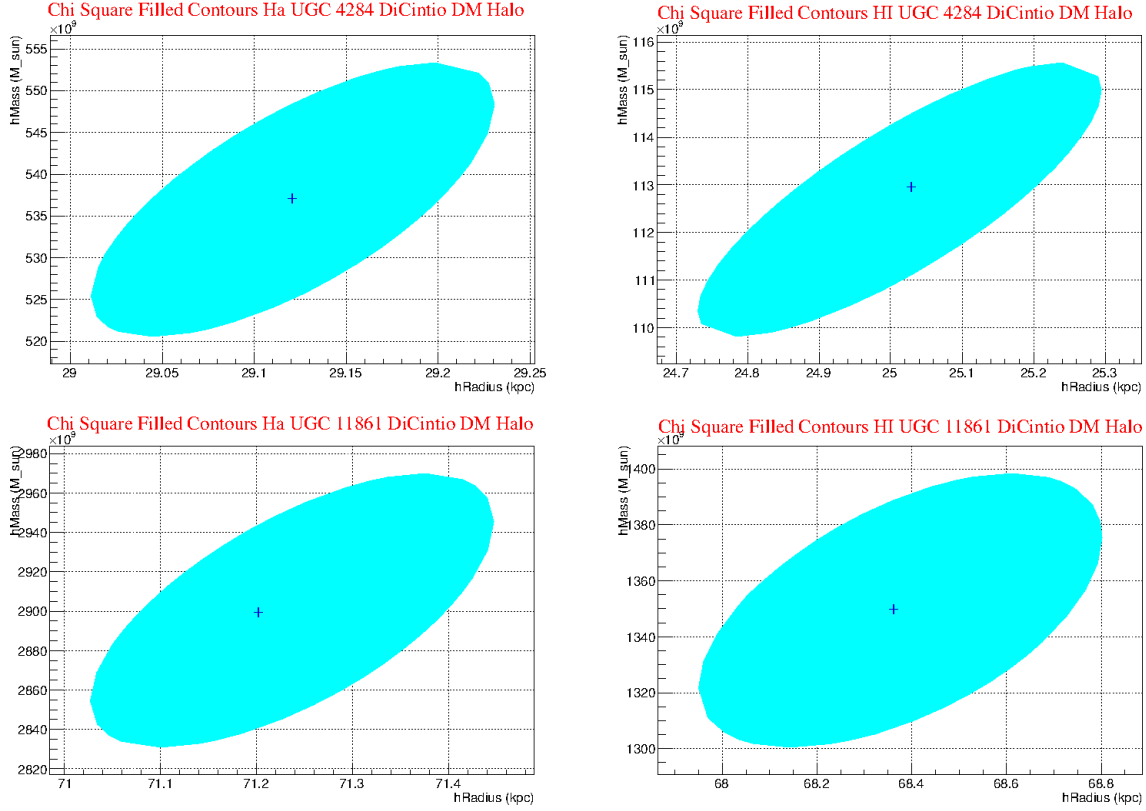


Figure 15. χ^2 filled contours at 70% confidence level. *First Panel:* H α DM RC of UGC 4284 DCH fit. *Second Panel:* HI DM RC of UGC 4284 DCH fit. *Third Panel:* H α DM RC of UGC 11861 DCH fit. *Fourth Panel:* HI DM RC of UGC 11861 DCH fit. The blue crosses represent the solutions found through the fitting procedure.

Table 3. H α DM RCs fit result for UGC 4284 (DOF=78).

UGC 4284 NFW	$M_d + 0\%^a$	$M_d - 30\%$	$M_d + 30\%$.
$M_h (M_\odot)$	7.07×10^{12}	3.75×10^{12}	3.98×10^{12}
$R_h (kpc)$	97.90	76.33	65.26
χ_r^{2b}	15.36	20.74	13.46
Edm ^c	1.45×10^9	1.30×10^9	1.70×10^9
UGC 4284 BKH	$M_d + 0\%$	$M_d - 30\%$	$M_d + 30\%$.
$M_h (M_\odot)$	3.63×10^9	2.91×10^9	4.52×10^9
$R_h (kpc)$	10.25	10.13	10.45
χ_r^2	8.94	12.72	5.99
Edm	1.22×10^{-13}	3.04×10^{-13}	1.74×10^{-13}
UGC 4284 DCH	$M_d + 0\%$	$M_d - 30\%$	$M_d + 30\%$.
$M_h (M_\odot)$	5.37×10^{11}	7.86×10^{11}	3.57×10^{11}
$R_h (kpc)$	29.12	36.15	22.53
χ_r^2	3.32	2.94	3.66
Edm	3.83×10^{-15}	7.09×10^{-14}	1.48×10^{-18}

^a $M_d = 7.92 \times 10^9 M_\odot$

^b Reduced χ^2

^c Estimated distance from the minimum

sired DM cored central profile (Governato et al. 2010, 2012; de Souza et al. 2011; Di Cintio et al. 2014).

Regardless of all the considerable observational and

theoretical endeavours to contribute to the solution of the cuspy/core controversy, the debate is still open and in this work we attempt to discriminate between cuspy and core DM halos through DM RCs fitting after subtracting from the observed RCs the stellar and gas rotational components. We consider high resolution H α and HI RCs of two irregular galaxies, UGC 4284 and UGC 11861, available in the literature, to examine the mass content of both objects by subtracting to the observed H α the stellar rotation velocity and to the HI RCs both the stellar and gas rotation velocity. We obtained the stellar rotational component through stellar population synthesis of the disk of these two galaxies. We recognise that in the case of both galaxies, once subtracted the determined stellar and gas rotation velocity, it is missing more than 50% of mass, for a stellar disk mass of $M_d = 7.92 \times 10^9 M_\odot$ in the case of UGC 4284 and more than 40% of mass for a stellar disk mass of $M_d = 5.38 \times 10^{10} M_\odot$ in the case of UGC 11861. We explored the possibility that DM could account for the missing mass in these galaxies, and we fitted the derived DM RCs with five DM models, namely the NFW DM halo, the BK DM halo, the DC DM halo, the HE DM halo and the HSD DM halo, to estimate the assumed DM contribution to the total mass of UGC 4284 and UGC 11861.

The cuspy DC DM halo fit better the H α DM RC of UGC 4284 than any other DM halos used in this study, in all the other cases, say HI RC of UGC 4284 and H α and HI RCs of UGC 11861, the cored DM models give a better fit to

Table 4. H α DM RCs fit result for UGC 11861 (DOF=43).

UGC 11861 NFW	$M_d + 0\%^a$	$M_d - 30\%$	$M_d + 30\%$.
$M_h(M_\odot)$	2.93×10^{12}	7.05×10^{12}	4.79×10^{12}
$R_h(kpc)$	54.26	97.91	65.27
χ_r^{2b}	70.86	75.67	55.67
Edm ^c	9.62×10^8	1.37×10^9	5.58×10^{10}
UGC 11861 BKH	$M_d + 0\%$	$M_d - 30\%$	$M_d + 30\%$.
$M_h(M_\odot)$	3.16×10^9	3.25×10^9	3.08×10^9
$R_h(kpc)$	9.16	10.21	8.29
χ_r^2	46.10	58.32	35.71
Edm	1.40×10^{-13}	3.01×10^{-12}	9.10×10^{-13}
UGC 11861 DCH	$M_d + 0\%$	$M_d - 30\%$	$M_d + 30\%$.
$M_h(M_\odot)$	2.89×10^{12}	4.09×10^{12}	1.96×10^{12}
$R_h(kpc)$	71.24	88.29	54.92
χ_r^2	32.08	42.26	25.65
Edm	2.40×10^{-13}	1.40×10^{-14}	6.03×10^{-13}

^a $M_d = 5.38 \times 10^{10} M_\odot$ ^b Reduced χ^2 ^c Estimated distance from the minimum**Table 5.** HI DM RCs fit result for UGC 4284 (DOF=22).

UGC 4284 NFW	$M_d + 0\%^a$	$M_d - 30\%$	$M_d + 30\%$.
$M_h(M_\odot)$	4.16×10^{12}	3.64×10^{12}	2.94×10^{12}
$R_h(kpc)$	97.90	97.90	79.03
χ_r^{2b}	305.74	299.16	307.61
Edm ^c	4.77×10^8	4.52×10^8	2.61×10^9
UGC 4284 BKH	$M_d + 0\%$	$M_d - 30\%$	$M_d + 30\%$.
$M_h(M_\odot)$	1.0×10^8	1.0×10^8	1.0×10^8
$R_h(kpc)$	1.73	1.85	1.62
χ_r^2	108.25	131.65	118.67
Edm	1.34×10^{-7}	2.68×10^{-7}	1.67×10^{-8}
UGC 4284 DCH	$M_d + 0\%$	$M_d - 30\%$	$M_d + 30\%$.
$M_h(M_\odot)$	1.13×10^{11}	1.26×10^{11}	9.83×10^{10}
$R_h(kpc)$	25.01	31.69	19.08
χ_r^2	82.96	103.41	77.54
Edm	3.18×10^{-14}	5.67×10^{-14}	2.67×10^{-14}

^a $M_d = 7.92 \times 10^9 M_\odot$ ^b Reduced χ^2 ^c Estimated distance from the minimum

the DM RCs of both galaxies than the cuspy DM profiles. In more detail the HE and HSD DM halos with two free parameters perform better than the BK DM halos except for the H α DM RC of UGC 4284 with stellar disk mass $M_d + 30\%$. The HE DM halo achieve better results than the HSD DM halo for the HI DM RCs of both galaxies and also for the DM H α RC of UGC 11861 with stellar disk mass $M_d + 0\%$ and $M_d + 30\%$. The HSD DM halo give better results than the HE for the DM H α RC of UGC 4284 and DM RC of UGC 11861 with stellar disk mass $M_d - 30\%$.

Table 6. HI DM RCs fit result for UGC 11861 (DOF=10).

UGC 11861 NFW	$M_d + 0\%^a$	$M_d - 30\%$	$M_d + 30\%$.
$M_h(M_\odot)$	5.46×10^{12}	6.24×10^{12}	3.89×10^{12}
$R_h(kpc)$	81.36	88.45	78.67
χ_r^{2b}	97.35	95.34	92.67
Edm ^c	3.28×10^8	5.32×10^8	6.54×10^8
UGC 11861 BKH	$M_d + 0\%$	$M_d - 30\%$	$M_d + 30\%$.
$M_h(M_\odot)$	6.53×10^8	6.12×10^8	6.94×10^8
$R_h(kpc)$	3.87	4.01	3.75
χ_r^2	37.60	38.35	36.93
Edm	2.13×10^{-13}	2.53×10^{-12}	1.89×10^{-12}
UGC 11861 DCH	$M_d + 0\%$	$M_d - 30\%$	$M_d + 30\%$.
$M_h(M_\odot)$	1.35×10^{12}	1.70×10^{12}	1.01×10^{12}
$R_h(kpc)$	68.38	85.26	52.22
χ_r^2	44.98	54.95	48.08
Edm	4.17×10^{-13}	3.59×10^{-15}	6.15×10^{-13}

^a $M_d = 5.38 \times 10^{10} M_\odot$ ^b Reduced χ^2 ^c Estimated distance from the minimum

As mentioned in section 6 the cuspy result we obtain in the case of the H α DM RC of UGC 4284 is in accordance with the numerical study of Di Cintio et al. (2014) (see figure 4 of that article), given that our range of stellar, DM halo masses and inner slopes coincide with those presented in the quoted figure. Another important outcome of this study is the fact that the M/L ratio is not constant in none of the two studied galaxies (see figures 3 and 4).

At this point we can answer, at least for UGC 4284 and UGC 11861, to the question we asked in the Introduction, i.e., if the DM profile slope could change substantially obtaining the stellar disk from stellar population studies instead of assuming a constant M/L as previous studies done in the past (see Introduction and references therein). From the results outlined above it seems that in the case of UGC 4284 and UGC 11861, the answer to this question is a negative one. In the future we plan to repeat this study for other high resolution RCs, in order to asses this question for a larger number of galaxies.

8 CONCLUSIONS

In this study we analyse the inner and outer mass distribution of the two irregular galaxies UGC 4284 and UGC 11861, by means of high resolution H α and HI RCs available in the literature. Additionally, we constrained the stellar content of UGC 4284 and UGC 11861 throughout stellar population synthesis studies, applied to the photometric observations of these two galaxies in several filters, we also derive *HI+He* RCs for the HI observed RCs of both galaxies and we subtracted the derived stellar disk from the observed H α RCs and the stellar and gas disk from the observed HI RCs.

We fitted the determined DM RCs for both galaxies, examining the NFW, BK, DC, HE and HSD DM models. The principal results of this research can be summarized

according to the following points:

(i) Cored DM models better fit the observed shape of the two DM $H\alpha$ and HI RCs considered in this study, with respect to cuspy DM models, except for the $H\alpha$ DM RC of UGC 4284 where the cuspy DC DM halo is the preferable model.

(ii) Cored exponential DM model Einasto reproduced better the DM HI RCs of UGC 4284, and UGC 11861, than the other models tested in this paper.

(iii) Cored exponential DM model Einasto reproduced better than all the other models the DM $H\alpha$ RCs of UGC 11861 for stellar masses $M_d + 0\%$ and $M_d + 30\%$.

(iv) The cored Stadel DM model, in the case of the $H\alpha$ DM RC of UGC 4284, performed better than Einasto DM models for all the stellar masses considered.

(v) The cored Stadel DM model, in the case of the $H\alpha$ DM RC of UGC 11861 and a stellar mass $M_d - 30\%$, achieved better results than Einasto DM models.

ACKNOWLEDGMENTS

RP acknowledges CNPq's financial support for postdoctoral fellowship at LNA. EMG acknowledges CONACYT's financial support for postdoctoral fellowship at INAOE. We also acknowledge the DGAPA-UNAM project IN 108912 and CONACYT-CB-2007/82389 project. We acknowledge Janine Van Eymeren for providing us the HI total density map of both galaxies.

REFERENCES

- Amram P., Adami C., Balkowski C., Blais-Ouellette S., Boselli A., Boulesteix J., Carignan C., 2002, *Ap&SS*, 281, 393
- Bahcall J. N., Schmidt M., Soneira R. M., 1982, *ApJL*, 258, L23
- Bell E. F., de Jong R. S., 2001, *ApJ*, 550, 212
- Bell E. F., McIntosh D. H., Katz N., Weinberg M. D., 2003, *ApJS*, 149, 289
- Blais-Ouellette S., Amram P., Carignan C., 2001, *AJ*, 121, 1952
- Blumenthal G. R., Faber S. M., Primack J. R., Rees M. J., 1984, *Natur*, 311, 517
- Bosma A., 1978, PhD thesis, Groningen Univ., (1978)
- Bosma A., 1981a, *AJ*, 86, 1791
- Bosma A., 1981b, *AJ*, 86, 1825
- Bruzual G., 2007, in Vallenari A., Tantaló R., Portinari L., Moretti A., eds, *From Stars to Galaxies: Building the Pieces to Build Up the Universe Vol. 374 of Astronomical Society of the Pacific Conference Series, Stellar Populations: High Spectral Resolution Libraries. Improved TP-AGB Treatment*. p. 303
- Bruzual G., Charlot S., 2003, *MNRAS*, 344, 1000
- Burkert A., 1995, *ApJL*, 447, L25
- Cabrera-Lavers A., Garzón F., 2004, *AJ*, 127, 1386
- Carignan C., Freeman K. C., 1985, *ApJ*, 294, 494
- Carignan C., Freeman K. C., 1988, *ApJL*, 332, L33
- Chabrier G., 2003, *PASP*, 115, 763
- Chapelon S., Contini T., Davoust E., 1999, *A&A*, 345, 81
- Chapman N. L., Mundy L. G., Lai S.-P., Evans II N. J., 2009, *ApJ*, 690, 496
- Charlot S., Fall S. M., 2000, *ApJ*, 539, 718
- Chemin L., de Blok W. J. G., Mamon G. A., 2011, *AJ*, 142, 109
- Ciotti L., Bertin G., 1999, *A&A*, 352, 447
- Coccatto L., Corsini E. M., Pizzella A., Morelli L., Funes J. G., Bertola F., 2004, *A&A*, 416, 507
- da Cunha E., Charlot S., Elbaz D., 2008, *MNRAS*, 388, 1595
- de Blok W. J. G., Bosma A., 2002, *A&A*, 385, 816
- de Blok W. J. G., McGaugh S. S., Rubin V. C., 2001, *AJ*, 122, 2396
- de Dénus-Baillargeon M.-M., Hernandez O., Boissier S., Amram P., Carignan C., 2013, *ApJ*, 773, 173
- de Souza R. S., Rodrigues L. F. S., Ishida E. E. O., Opher R., 2011, *MNRAS*, 415, 2969
- de Vaucouleurs G., de Vaucouleurs A., Corwin Jr. H. G., Buta R. J., Paturel G., Fouque P., 1991, *S&T*, 82, 621
- Di Cintio A., Brook C. B., Dutton A. A., Macciò A. V., Stinson G. S., Knebe A., 2014, *MNRAS*, 441, 2986
- Di Cintio A., Brook C. B., Macciò A. V., Stinson G. S., Knebe A., Dutton A. A., Wadsley J., 2014, *MNRAS*, 437, 415
- Dutton A. A., Courteau S., de Jong R., Carignan C., 2005, *ApJ*, 619, 218
- Dutton A. A., Macciò A. V., 2014, *MNRAS*, 441, 3359
- Einasto J., 1965, *Trudy Astrofizicheskogo Instituta Alma-Ata*, 5, 87
- Epinat B., Amram P., Marcelin M., 2008, *MNRAS*, 390, 466
- Ferrers N. M., 1877, *QJPAM*, 14, 1
- Freeman K. C., 1970, *ApJ*, 160, 811
- Fuentes-Carrera I., Rosado M., Amram P., Salo H., Laurikainen E., 2007, *A&A*, 466, 847
- Gallazzi A., Bell E. F., 2009, *ApJS*, 185, 253
- Gallazzi A., Brinchmann J., Charlot S., White S. D. M., 2008, *MNRAS*, 383, 1439
- Gallazzi A., Charlot S., Brinchmann J., White S. D. M., Tremonti C. A., 2005, *MNRAS*, 362, 41
- Garrido O., Marcelin M., Amram P., 2004, *MNRAS*, 349, 225
- Garrido O., Marcelin M., Amram P., Balkowski C., Gach J. L., Boulesteix J., 2005, *MNRAS*, 362, 127
- Garrido O., Marcelin M., Amram P., Boissin O., 2003, *A&A*, 399, 51
- Garrido O., Marcelin M., Amram P., Boulesteix J., 2002, *A&A*, 387, 821
- Governato F., Brook C., Mayer L., Brooks A., Rhee G., Wadsley J., Jonsson P., Willman B., Stinson G., Quinn T., Madau P., 2010, *Natur*, 463, 203
- Governato F., Zolotov A., Pontzen A., Christensen 2012, *MNRAS*, 422, 1231
- Gradshteyn I. S., Ryzhik I. M., 2007, *Table of integrals, series, and products*, seventh edn. Elsevier/Academic Press, Amsterdam
- Jobin M., Carignan C., 1990, *AJ*, 100, 648

Józsa G. I. G., 2007, *A&A*, 468, 903
 Kandalian R. A., Kalloghlian A. T., 1998, *Astrophysics*, 41, 1
 Kennicutt Jr. R. C., Armus L., Bendo G., Calzetti D., Dale D. A., Draine B. T., Engelbracht 2003, *PASP*, 115, 928
 Kuzio de Naray R., McGaugh S. S., de Blok W. J. G., 2008, *ApJ*, 676, 920
 Kuzio de Naray R., McGaugh S. S., de Blok W. J. G., Bosma A., 2006, *ApJS*, 165, 461
 MacArthur L. A., 2005, *ApJ*, 623, 795
 Marigo P., Girardi L., 2007, *A&A*, 469, 239
 Marigo P., Girardi L., Bressan A., Groenewegen M. A. T., Silva L., Granato G. L., 2008, *A&A*, 482, 883
 Martinbeau N., Carignan C., Roy J.-R., 1994, *AJ*, 107, 543
 Navarro J. F., Frenk C. S., White S. D. M., 1996, *ApJ*, 462, 563
 Navarro J. F., Hayashi E., Power C., Jenkins A. R., Frenk C. S., White S. D. M., Springel V., Stadel J., Quinn T. R., 2004, *MNRAS*, 349, 1039
 Navarro J. F., Ludlow A., Springel V., Wang J., Vogelsberger M., White S. D. M., Jenkins A., Frenk C. S., Helmi A., 2010, *MNRAS*, 402, 21
 Paturel G., Petit C., Prugniel P., Theureau G., Rousseau J., Brouty M., Dubois P., Cambrésy L., 2003, *A&A*, 412, 45
 Peng C. Y., Ho L. C., Impey C. D., Rix H.-W., 2002, *AJ*, 124, 266
 Peng C. Y., Ho L. C., Impey C. D., Rix H.-W., 2010, *AJ*, 139, 2097
 Persic M., Salucci P., 1990, *MNRAS*, 245, 577
 Persic M., Salucci P., Stel F., 1996, *MNRAS*, 281, 27
 Ratnam C., Salucci P., 2000, *NewA*, 5, 427
 Repetto P., Martínez-García E. E., Rosado M., Gabbasov R., 2013, *ApJ*, 765, 7
 Repetto P., Rosado M., Gabbasov R., Fuentes-Carrera I., 2010, *AJ*, 139, 1600
 Rubin V. C., Ford W. K. J., Thonnard N., 1980, *ApJ*, 238, 471
 Salucci P., Yegorova I. A., Drory N., 2008, *MNRAS*, 388, 159
 Schlafly E. F., Finkbeiner D. P., 2011, *ApJ*, 737, 103
 Sheth K., Regan M., Hinz J. L., Gil de Paz A., Menéndez-Delmestre K., Muñoz-Mateos 2010, *PASP*, 122, 1397
 Spano M., Marcelin M., Amram P., Carignan C., Epinat B., Hernandez O., 2008, *MNRAS*, 383, 297
 Stadel J., Potter D., Moore B., Diemand J., Madau P., Zemp M., Kuhlen M., Quilis V., 2009, *MNRAS*, 398, L21
 Swaters R. A., Madore B. F., Trewella M., 2000, *ApJL*, 531, L107
 Swaters R. A., Madore B. F., van den Bosch F. C., Balcells M., 2003, *ApJ*, 583, 732
 van Albada T. S., Bahcall J. N., Begeman K., Sancisi R., 1985, *ApJ*, 295, 305
 van Albada T. S., Sancisi R., 1986, *Royal Society of London Philosophical Transactions Series A*, 320, 447
 van Eymeren J., Jütte E., Jog C. J., Stein Y., Dettmar R.-J., 2011, *A&A*, 530, A29
 Verheijen M. A. W., Sancisi R., 2001, *A&A*, 370, 765
 Zhao H., 1996, *MNRAS*, 278, 488
 Zibetti S., Charlot S., Rix H.-W., 2009, *MNRAS*, 400, 1181

APPENDIX A: EINASTO AND STADEL DM RC FIT RESULTS

We also consider the Einasto (HE) (Einasto 1965) and the Stadel (Stadel et al. 2009) (HSD) DM velocity profiles in our endeavour to reproduce the H α and HI DM RCs of UGC 4284 and UGC 11861. The motivation to employ the HE and HSD DM halos are emphasized below, even if at the moment it does not exist a physical justification of these two DM profiles. During the fitting process we fixed the third parameter of both DM halos, therefore the number of degrees of freedom is the same of the other DM halos examined in this work.

The HE was introduced for the first time by Einasto (1965) to build a model of the distribution of stars in the Galaxy. Navarro et al. (2004, 2010) established that the HE fits the DM density profiles produced in the framework of Λ CDM cosmological numerical simulations better than the NFW profile. Chemin et al. (2011) used for the first time the HE DM models to fit 34 nearby galaxies, determining that the HE DM halo represented better the observed RCs of the studied galaxies than the Pseudo-Isothermal DM model.

The HE represents a three parameters model in the form of an exponential-like profile and also incorporates cusped and cored DM halos. We used the approximation of Ciotti & Bertin (1999) for the dimensionless scale factor d_n .

The HSD have been proposed by Stadel et al. (2009) accomplishing several Λ CDM Galactic mass DM halo numerical simulations, the authors concluded that the HSD better reproduced the shape of the simulated DM halos density profiles also if compared with the HE. The HSD is an exponential-like profile with three free parameters, but according to Stadel et al. (2009) can also be regarded as a DM density profile with two free parameters with functional form:

$$\rho(r) = \rho_0 e^{-\lambda[\ln(1+r/R_\lambda)]^2},$$

where R_λ is the HSD scale radius and λ is a parameter that governs the shape of the HSD. In this study we also provide an exact derivation of the HSD velocity profile in Appendix B. In particular the relation (B10) of Appendix B, is a tabulated integral from Gradshteyn & Ryzhik (2007). The relation (B19) of the same Appendix B, is the expression we used in this investigation to fit the DM RCs of UGC 4284 and UGC 11861 employing the HSD. The results of the HE and HSD fits are listed in table A1 and table A2.

APPENDIX B: CIRCULAR VELOCITY DERIVATION FOR THE STADEL DM MODEL

The spatial density relation for the HSD halo density profile is expressed by the relation:

$$\rho(r) = \rho_0 e^{-\lambda[\ln(1+\frac{r}{R_\lambda})]^2}. \quad (\text{B1})$$

We can write this spatial density in the following form:

$$\rho(r) = \rho_0 \left[e^{\ln(1+\frac{r}{R_\lambda})} \right]^{-\lambda \ln(1+\frac{r}{R_\lambda})}, \quad (\text{B2})$$

Table A1. H α DM RC fit results (UGC 4284 DOF=78 AND UGC 11861 DOF=43).

UGC 4284 EINASTO	$M_d + 0\%$	$M_d - 30\%$	$M_d + 30\%$.
$M_h(M_\odot)$	1.22×10^{12}	1.26×10^{12}	1.22×10^{12}
$R_h(kpc)$	100	100	100
n_h	3.16	2.92	3.37
χ_r^2	4.43	4.04	4.96
Edm	8.37×10^{-8}	2.40×10^{-7}	4.10×10^{-7}
UGC 4284 STADEL	$M_d + 0\%$	$M_d - 30\%$	$M_d + 30\%$.
$M_h(M_\odot)$	8.70×10^{11}	1.14×10^{12}	5.17×10^{11}
$R_h(kpc)$	47.13	59.65	33.73
λ_h	3.79	3.80	3.81
χ_r^2	6.13	7.10	8.77
Edm	1.07×10^{-11}	1.61×10^{-14}	6.39×10^{-9}
UGC 11861 EINASTO	$M_d + 0\%$	$M_d - 30\%$	$M_d + 30\%$.
$M_h(M_\odot)$	1.19×10^{11}	8.27×10^{10}	1.81×10^{11}
$R_h(kpc)$	14.92	12.85	18.12
n_h	1.13	0.92	1.39
χ_r^2	6.18	10.04	3.74
Edm	3.81×10^{-14}	1.68×10^{-13}	3.88×10^{-16}
UGC 11861 STADEL	$M_d + 0\%$	$M_d - 30\%$	$M_d + 30\%$.
$M_h(M_\odot)$	5.27×10^{11}	4.61×10^{11}	9.86×10^{11}
$R_h(kpc)$	31.23	31.22	41.89
λ_h	3.65	3.59	3.75
χ_r^2	8.05	8.02	8.96
Edm	1.74×10^{-13}	2.70×10^{-16}	4.11×10^{-8}

Table A2. HI DM RC fit results (UGC 4284 DOF=22 AND UGC 11861 DOF=10).

UGC 4284 EINASTO	$M_d + 0\%$	$M_d - 30\%$	$M_d + 30\%$.
$M_h(M_\odot)$	1.82×10^{10}	1.59×10^{10}	2.06×10^{10}
$R_h(kpc)$	5.42	5.23	5.64
n_h	0.80	0.73	0.87
χ_r^2	5.90	5.74	6.10
Edm	1.68×10^{-15}	1.59×10^{-15}	5.99×10^{-16}
UGC 4284 STADEL	$M_d + 0\%$	$M_d - 30\%$	$M_d + 30\%$.
$M_h(M_\odot)$	7.41×10^{10}	6.44×10^{10}	8.02×10^{10}
$R_h(kpc)$	12.18	11.60	11.84
λ_h	3.82	3.77	3.73
χ_r^2	25.30	24.33	17.95
Edm	3.52×10^{-12}	4.78×10^{-12}	1.68×10^{-14}
UGC 11861 EINASTO	$M_d + 0\%$	$M_d - 30\%$	$M_d + 30\%$.
$M_h(M_\odot)$	5.70×10^{10}	5.16×10^{10}	6.54×10^{10}
$R_h(kpc)$	9.20	10.30	11.40
n_h	1.12	1.10	1.15
χ_r^2	19.50	17.25	20.51
Edm	1.26×10^{-8}	1.30×10^{-9}	1.17×10^{-9}
UGC 11861 STADEL	$M_d + 0\%$	$M_d - 30\%$	$M_d + 30\%$.
$M_h(M_\odot)$	3.65×10^{11}	3.31×10^{11}	4.0×10^{11}
$R_h(kpc)$	26.60	27.04	26.18
λ_h	3.79	3.79	3.79
χ_r^2	26.70	31.38	27.98
Edm	2.06×10^{-14}	1.44×10^{-13}	1.21×10^{-14}

using exponential properties we obtain the relation:

$$\rho(r) = \rho_0 \left[\frac{1}{\left(1 + \frac{r}{R_\lambda}\right)^\lambda} \right]^{\ln\left(1 + \frac{r}{R_\lambda}\right)} \quad (\text{B3})$$

thus we can use this form of the spatial density to obtain the mass density up to a radius r , with the relation:

$$M(r) = 4\pi \int_0^r \rho(s) s^2 ds \quad (\text{B4})$$

substituting in this relation we obtain:

$$M(r) = 4\pi \rho_0 \int_0^r \left[\frac{1}{\left(1 + \frac{s}{R_\lambda}\right)^\lambda} \right]^{\ln\left(1 + \frac{s}{R_\lambda}\right)} s^2 ds \quad (\text{B5})$$

with the substitution $e^u = \frac{1}{\left(1 + \frac{s}{R_\lambda}\right)^\lambda} \Rightarrow e^{\frac{u}{\lambda}} = \frac{1}{\left(1 + \frac{s}{R_\lambda}\right)}$

we obtain $s = R_\lambda \left(\frac{1 - e^{\frac{u}{\lambda}}}{e^{\frac{u}{\lambda}}} \right) \Rightarrow s = R_\lambda \left(e^{-\frac{u}{\lambda}} - 1 \right)$ and $u = -\lambda \ln \left(1 + \frac{s}{R_\lambda} \right) \Rightarrow du = -\lambda \frac{ds}{R_\lambda} \ln \left(1 + \frac{s}{R_\lambda} \right) \Rightarrow du = -\lambda \frac{1}{\left(1 + \frac{s}{R_\lambda}\right)} ds \Rightarrow du = -\frac{\lambda}{R_\lambda} e^{\frac{u}{\lambda}} ds \Rightarrow ds = -\frac{R_\lambda}{\lambda} e^{-\frac{u}{\lambda}} du$.

For the limits of integration we have that $u = \ln \left[\frac{1}{\left(1 + \frac{r}{R_\lambda}\right)^\lambda} \right]$

we obtain $u = 0$ for $r = 0$ and $u = \ln \left[\frac{1}{\left(1 + \frac{r}{R_\lambda}\right)^\lambda} \right]$ for $r = r$.

It is important to note that the upper integration limit is negative given that $u = \ln \left[\left(1 + \frac{r}{R_\lambda}\right)^{-\lambda} \right] \Rightarrow u = -\lambda \ln \left[\left(1 + \frac{r}{R_\lambda}\right) \right]$ with $(\lambda, r, R_\lambda) > 0$.

We proceed in the calculation of the integral substituting all the derived quantities in the above relation obtaining:

$$M(r) = -\frac{4\pi\rho_0 R_\lambda^3}{\lambda} \int_0^{(u<0)} e^{-\frac{s^2}{\lambda}} \left(e^{-\frac{s}{\lambda}} - 1 \right)^2 e^{-\frac{s}{\lambda}} ds \quad (\text{B6})$$

After simplifying this relation and making the square we obtain the following relation:

$$M(r) = \frac{4\pi\rho_0 R_\lambda^3}{\lambda} \int_{(u<0)}^0 e^{-\frac{s^2}{\lambda}} \left(e^{-\frac{3s}{\lambda}} + e^{-\frac{s}{\lambda}} - 2e^{-\frac{2s}{\lambda}} \right) ds \quad (\text{B7})$$

multiplying and simplifying we get the expression:

$$M(r) = \frac{4\pi\rho_0 R_\lambda^3}{\lambda} \int_{(u<0)}^0 \left[e^{-\left(\frac{s^2+3s}{\lambda}\right)} + e^{-\left(\frac{s^2+s}{\lambda}\right)} - 2e^{-\left(\frac{s^2+2s}{\lambda}\right)} \right] ds \quad (\text{B8})$$

naming the first integral in the above expression as $A(s) = \int_{(u<0)}^0 e^{-\left(\frac{s^2+3s}{\lambda}\right)} ds$, the second $B(s) = \int_{(u<0)}^0 e^{-\left(\frac{s^2+s}{\lambda}\right)} ds$ and the third integral $C(s) = \int_{(u<0)}^0 e^{-\left(\frac{s^2+2s}{\lambda}\right)} ds$ we can rewrite our mass integral in the following manner:

$$M(r) = \frac{4\pi\rho_0 R_\lambda^3}{\lambda} [A(s) + B(s) - 2C(s)] \quad (\text{B9})$$

At this point considering each integral separately and considering the indefinite integral given by the expression:

$$\int e^{-(ax^2+2bx+c)} dx = \frac{1}{2} \sqrt{\frac{\pi}{a}} \exp\left(\frac{ac-b^2}{a}\right) \operatorname{erf}\left[\sqrt{a}x + \frac{b}{\sqrt{a}}\right] \quad (\text{B10})$$

where the $\operatorname{erf}(x)$ is given by relation $\operatorname{erf}(x) = \frac{2}{\sqrt{\pi}} \int_0^x e^{-t^2} dt$,

in the case of the first integral $A(s)$, we obtain $a = \frac{1}{\lambda}$; $b = \frac{3}{2\lambda}$. For the second integral $B(s)$ in a similar way we get $a = \frac{1}{\lambda}$; $b = \frac{1}{2\lambda}$ and for the third integral we obtain $a = \frac{1}{\lambda}$; $b = \frac{1}{\lambda}$. All the integrals have $c = 0$.

Thus the previously indefinite integrals $A(s)$, $B(s)$ and $C(s)$ transform according to the relation:

$$A(s) = \int e^{-\left(\frac{s^2+3s}{\lambda}\right)} ds = \frac{\sqrt{\pi\lambda}}{2} \exp\left(-\frac{9}{4\lambda}\right) \operatorname{erf}\left[\sqrt{\frac{1}{\lambda}}s + \frac{3}{2\sqrt{\lambda}}\right] \quad (\text{B11})$$

$$B(s) = \int e^{-\left(\frac{s^2+s}{\lambda}\right)} ds = \frac{\sqrt{\pi\lambda}}{2} \exp\left(-\frac{1}{4\lambda}\right) \operatorname{erf}\left[\sqrt{\frac{1}{\lambda}}s + \frac{1}{2\sqrt{\lambda}}\right] \quad (\text{B12})$$

$$C(s) = \int e^{-\left(\frac{s^2+2s}{\lambda}\right)} ds = \frac{\sqrt{\pi\lambda}}{2} \exp\left(-\frac{1}{\lambda}\right) \operatorname{erf}\left[\sqrt{\frac{1}{\lambda}}s + \frac{1}{\sqrt{\lambda}}\right] \quad (\text{B13})$$

now, we calculate the definite integrals setting $u = -v$ where $v > 0$ with the reminder that $\operatorname{erf}(-x) = -\operatorname{erf}(x)$ we obtain the following results:

$$\int_{(-v<0)}^0 e^{-\left(\frac{s^2+3s}{\lambda}\right)} ds = A(0) - A(-v) = \frac{\sqrt{\pi\lambda}}{2} \exp\left(-\frac{9}{4\lambda}\right) \times \left\{ \operatorname{erf}\left[\sqrt{\frac{1}{\lambda}}v - \frac{3}{2\sqrt{\lambda}}\right] + \operatorname{erf}\left[\frac{3}{2\sqrt{\lambda}}\right] \right\}$$

$$\int_{(-v<0)}^0 e^{-\left(\frac{s^2+s}{\lambda}\right)} ds = B(0) - B(-v) = \frac{\sqrt{\pi\lambda}}{2} \exp\left(-\frac{1}{4\lambda}\right) \times \left\{ \operatorname{erf}\left[\sqrt{\frac{1}{\lambda}}v - \frac{1}{2\sqrt{\lambda}}\right] + \operatorname{erf}\left[\frac{1}{2\sqrt{\lambda}}\right] \right\}$$

$$\int_{(-v<0)}^0 e^{-\left(\frac{s^2+2s}{\lambda}\right)} ds = C(0) - C(-v) = \frac{\sqrt{\pi\lambda}}{2} \exp\left(-\frac{1}{\lambda}\right) \times \left\{ \operatorname{erf}\left[\sqrt{\frac{1}{\lambda}}v - \frac{1}{\sqrt{\lambda}}\right] + \operatorname{erf}\left[\frac{1}{\sqrt{\lambda}}\right] \right\}$$

Let us define the part involving the erf functions in the above expressions in the following way:

$$I_{erf1}(v, \lambda) = \left\{ \operatorname{erf}\left[\sqrt{\frac{1}{\lambda}}v - \frac{3}{2\sqrt{\lambda}}\right] + \operatorname{erf}\left[\frac{3}{2\sqrt{\lambda}}\right] \right\} \quad (\text{B14})$$

$$I_{erf2}(v, \lambda) = \left\{ \operatorname{erf}\left[\sqrt{\frac{1}{\lambda}}v - \frac{1}{2\sqrt{\lambda}}\right] + \operatorname{erf}\left[\frac{1}{2\sqrt{\lambda}}\right] \right\} \quad (\text{B15})$$

$$I_{erf3}(v, \lambda) = \left\{ \operatorname{erf} \left[\sqrt{\frac{1}{\lambda}} v - \frac{1}{\sqrt{\lambda}} \right] + \operatorname{erf} \left[\frac{1}{\sqrt{\lambda}} \right] \right\} \quad (\text{B16})$$

at this point we can rewrite the HSD mass function in the following form:

$$M(r) = \frac{2\pi^{3/2}\rho_0 R_\lambda^3}{\lambda^{1/2}} \left[e^{-\frac{9}{4\lambda}} I_{erf1}(v, \lambda) + e^{-\frac{1}{4\lambda}} I_{erf2}(v, \lambda) - 2e^{-\frac{1}{\lambda}} I_{erf3}(v, \lambda) \right] \quad (\text{B17})$$

where $-v = \ln \frac{1}{\left(1 + \frac{r}{R_\lambda}\right)^\lambda}$ and the circular velocity is given by $V_c(r) = GM(r)/r$ so the above relation becomes:

$$V_c^2(r) = \frac{2\pi^{3/2}G\rho_0 R_\lambda^3}{\lambda^{1/2}r} \left[e^{-\frac{9}{4\lambda}} I_{erf1}(v, \lambda) + e^{-\frac{1}{4\lambda}} I_{erf2}(v, \lambda) - 2e^{-\frac{1}{\lambda}} I_{erf3}(v, \lambda) \right] \quad (\text{B18})$$

we can express the circular velocity expression as a function of the initial mass of the system remembering that $M_\lambda = \rho_0 V_\lambda$, where $V_\lambda = \frac{4}{3}\pi R_\lambda^3$ is the volume of a sphere of radius r containing the mass M for definition, so we obtain:

$$V_c^2(r) = \frac{3M_\lambda \pi^{1/2} G}{2\lambda^{1/2} r} \left[e^{-\frac{9}{4\lambda}} I_{erf1}(v, \lambda) + e^{-\frac{1}{4\lambda}} I_{erf2}(v, \lambda) - 2e^{-\frac{1}{\lambda}} I_{erf3}(v, \lambda) \right] \quad (\text{B19})$$

where $M_\lambda = \frac{4}{3}\pi R_\lambda^3 \rho_0$ is the mass enclosing the initial density ρ_0 inside a radius R_λ and G is the gravitational constant expressed in astrophysical units ($M_\odot^{-1} \text{ kpc km}^2 \text{ s}^{-2}$).